Multi-omics profiling establishes the polypharmacology of FDA Approved CDK4/6 inhibitors and its impact on drug response

Marc Hafner*[,1,3], Caitlin E. Mills*[,1], Kartik Subramanian[1], Chen Chen[1], Mirra Chung[1], Sarah A. Boswell[1], Robert A. Everley[1], Changchang Liu[1], Charlotte S. Walmsley[2], Dejan Juric[1,2,ϕ], and Peter K. Sorger[1,†,ϕ]

* These authors contributed equally to this work.
ϕ These authors contributed equally to this work.

† Lead contact: Peter Sorger (peter_sorger@hms.harvard.edu, 617-432-6901/6902); orcid.org/0000-0002-3364-1838 copying Chris Bird (christopher_bird@hms.harvard.edu).

[1]Laboratory of Systems Pharmacology
Department of Systems Biology
Harvard Medical School
Boston, MA 02115

[2]Termeer Center for Targeted Therapies
Massachusetts General Hospital Cancer Center
Boston, MA 02114

[3]Current address:
Department of Bioinformatics & Computational Biology
Genentech, Inc.
South San Francisco, CA 94080

M. Hafner is currently an employee of Genentech, Inc and declares no conflicts of interest. R. Everley is currently an employee of Pfizer, Inc and declares no conflicts of interest. Other authors have no conflict of interest.

Key words: Targeted therapy; HR+ breast cancer; CDK4/6 inhibitors; drug profiling; drug mechanisms of action

Running title: Advantageous polypharmacology of CDK4/6 inhibitors

SUMMARY

FDA approval of multiple drugs differing in chemical structures but targeting the same protein raises the question whether such drugs have sufficiently similar mechanisms of action to be considered functionally equivalent. In this paper we compare three recently approved inhibitors of the cyclin-dependent kinases CDK4/6 – palbociclib, ribociclib, and abemaciclib – that are becoming important therapies for the treatment of hormone-receptor positive breast and potentially other cancers. We find that transcriptional and proteomic changes induced by the three drugs differ significantly and that abemaciclib has unique cellular activities including induction of cell death (even in pRb-deficient cells), arrest in the G2 phase of the cell cycle, and reduced drug adaptation. These activities appear to arise from inhibition of kinases other than CDK4/6 including CDK2/Cyclin A/E and CDK1/Cyclin B.

SIGNIFICANCE

The target profiles of most drugs are established relatively early in their development and are not systematically revisited at the time of approval. Scattered reports suggest that palbociclib, ribociclib, and abemaciclib differ in pharmacokinetics, dosing, and adverse effects but the three drugs are generally regarded as similar. Our finding that the drugs differ substantially in mechanism of action – abemaciclib retains activities of the earlier-generation drug alvocidib – suggests the potential for different uses in the clinic: in particular, abemaciclib may show activity in patients progressing on palbociclib or ribociclib. More generally, our approach relying on data from five distinct phenotypic and biochemical assays strongly suggests that a multi-faceted approach is necessary to get a reliable picture the target spectrum of kinase inhibitors.

INTRODUCTION

Progression through the cell cycle is controlled by over a dozen distinct protein complexes involving cyclins and cyclin-dependent kinases (CDKs). Because dysregulation of the cell cycle is a hallmark of cancer, several generations of CDK inhibitors have been tested as potential therapeutic agents. However, developing CDK inhibitors that are more active on tumor than normal cells has been a challenge and it is only recently that CDK4/6 inhibitors have emerged as promising therapies, particularly in breast cancer. CDK4 and CDK6 bind cyclin D early in the G1 phase of the cell cycle and phosphorylate the retinoblastoma protein (pRb). pRb is then hyper-phosphorylated by CDK2/cyclin E, relieving its inhibitory activities against transcription factors of the E2F family and allowing for S phase entry. Later in the cell cycle, CDK2/cyclin A and CDK1 in complex with cyclin A and B promote entry and progression through G2 and mitosis. Multiple genetic changes in cancer cells disrupt critical steps in cell cycle regulation: amplification of CDK4, CDK6, cyclin D, or cyclin E are common in solid tumors including breast cancers (Balko *et al.*, 2014; Asghar *et al.*, 2015). Deficiencies in pRb function, which cause unregulated S phase entry, as well as deletion of the CDK4/6 inhibitor p16 (encoded by *CDKN2A*) are also common (Franco, Witkiewicz and Knudsen, 2014; Asghar *et al.*, 2015).

First generation pan-CDK inhibitors active against cell cycle regulators such as CDK1/2/4/6 and transcriptional regulators such as CDK9 arrest cells in both G1 and G2 and were found to be broadly cytotoxic (Asghar *et al.*, 2015). Clinical development of these CDK inhibitors has been challenging largely because of poor therapeutic windows (Asghar *et al.*, 2015) thought to arise from a lack of selectivity for specific CDKs. Subsequent generations of CDK inhibitors were therefore designed to inhibit subsets of CDK proteins. In February 2015, the CDK4/6 inhibitor, palbociclib (PD0332991; Ibrance®) (Cristofanilli *et al.*, 2016) received FDA approval for management of hormone receptor-positive (HR^+) metastatic breast cancer (MBC) (Finn *et al.*, 2009; O'Leary, Finn and Turner, 2016). Subsequent clinical trials of the CDK4/6 inhibitors, ribociclib (LEE011; KISQALI®) (Hortobagyi *et al.*, 2016) and abemaciclib (LY2835219; Verzenio®) (Dickler *et al.*, 2016; Sledge *et al.*, 2017) also

demonstrated substantial improvements in progression-free survival in HR^+ metastatic breast cancer (Cristofanilli *et al.*, 2016; Griggs and Wolff, 2017) leading to their FDA approval. CDK4/6 inhibitors are currently regarded as some of the most promising new drugs for the treatment of HR^+ breast cancer and are also being tested against other malignancies (McCain, 2015; Goel *et al.*, 2016; Lim, Turner and Yap, 2016; Patnaik, Lee S. Rosen, *et al.*, 2016).

As observed with many other targeted therapies, however, acquired resistance to CDK4/6 inhibitors develops over time and nearly all initially responsive patients ultimately progress (Sherr, Beach and Shapiro, 2016). Resistance to CDK4/6 inhibitors is associated with multiple genomic alterations including amplification of Cyclin E, which promotes CDK2-dependent phosphorylation of pRb, amplification of CDK6, and loss of pRb function (Asghar *et al.*, 2015; Yang *et al.*, 2017). High expression of cyclin E is also associated with high CDK2 activity post-mitosis, which appears to bypass a requirement for CDK4/6 for cell cycle reentry (Asghar *et al.*, 2017).

Despite having the same nominal targets and similar initial clinical indications, emerging evidence suggests that palbociclib, ribociclib, and abemaciclib differ in the clinic: abemaciclib in particular has been reported to have single-agent activities and distinct adverse effects (Patnaik, Lee. S Rosen, *et al.*, 2016; O'Brien *et al.*, 2018). The three drugs are dosed differently, have different pharmacokinetics, and are reported to differ with respect to target selectivity (Kim *et al.*, 2013; Gelbert *et al.*, 2014; Chen, N. V. Lee, *et al.*, 2016; Cousins *et al.*, 2017). Among abemaciclib secondary targets examined to date, inhibition of DYRK/HIPK kinases is thought to contribute to cellular cytotoxicity (Knudsen *et al.*, 2017); inhibition of GSK3α/β can activate WNT signaling (Cousins *et al.*, 2017); but inhibition of CDK9 is thought to be therapeutically unimportant (Torres-guzmán *et al.*, 2017); Overall, however, the significance of differences in potency against CDK4/6 vs. other targets remains largely unexplored.

The target profiles of most clinical compounds are established relatively early in their development and are not necessarily revised at the time of approval. This is further complicated in the

case of kinase inhibitors by the use of different measurement technologies and the steady evolution of these technologies over the course of drug development. By directly comparing the target profiles and biological activities of palbociclib, ribociclib and abemaciclib, as well as an earlier generation pan-CDK inhibitor alvocidib (flavopiridol), we sought to address three questions: (i) are the three approved CDK4/6 inhibitors interchangeable with respect to biochemical and cell-based activities; (ii) is there a possibility that tumors that have become resistant to one CDK4/6 inhibitor might remain responsive to another inhibitor; and (iii) what are the relative merits of different approaches to characterizing the target spectrum of kinase inhibitors?

In this paper we report the analysis of CDK4/6 inhibitors using five experimental approaches that provide complementary insights into drug mechanisms of action: (i) mRNA sequencing of drug-perturbed cells, (ii) phosphoproteomics using mass spectrometry, (iii) GR-based dose-response measurement of cellular phenotypes (Hafner *et al.*, 2016), (iv) mRNA sequencing of drug-treated xenograft tumors and (v) three distinct types of *in vitro* analysis (activity assays with recombinant enzymes; kinome-wide profiling using the commercial KINOMEscan platform from DiscoverX (Fabian *et al.*, 2005); and kinase enrichment proteomics based on affinity purification on kinobeads (Duncan *et al.*, 2012). We find that the five experimental approaches provide different but complementary views of target coverage and demonstrate that palbociclib, ribociclib, and abemaciclib have differences in secondary targets and biological activities in breast cancer cell lines of varying genotypes. Multiple lines of evidence, including an *in vivo* xenograft model, show that the biological activities of abemaciclib arise from inhibition of kinases in addition to CDK4/6, notably CDK1/cyclin B and CDK2/cyclin E.

RESULTS

Approved CDK4/6 inhibitors induce distinct molecular signatures in breast cancer cells

To compare the mechanisms of action of palbociclib, ribociclib, and abemaciclib we performed transcriptional profiling (mRNA-seq) on a panel of seven breast cancer cell lines following 6 or 24 hours

of exposure to 0.3, 1 or 3 μM of drug (Figure 1a and Table S1). In all but pRb-deficient BT-549 cells, treatment with any of the three drugs gave rise to a signature (signature 1; Figure 1a in red) comprising 87 significantly down-regulated genes (FDR < 0.2). In addition, treatment of cells with abemaciclib in the low micromolar range induced a second transcriptional signature (signature 2; Figure 1a in cyan) that was absent from ribociclib-exposed cells and only weakly present in cells exposed to palbociclib. We queried the Broad Connectivity Map (CMAP) (Lamb *et al.*, 2006) with the two sets of down-regulated genes to determine which drug-induced changes they most closely matched. For signature 1, palbociclib and inhibitors of MEK (MAP kinase kinase) were the strongest hits (ribociclib and abemaciclib are absent from the CMAP dataset; Figure 1b and Table S2). Like CDK4/6 inhibition, MEK inhibition is anti-mitogenic in breast cancer cells, causing them to arrest at the G1/S transition (Meloche and Pouysségur, 2007; Caunt *et al.*, 2015). Gene set enrichment analysis showed that signature 1 was enriched for genes in the set *Reactome "Cell Cycle"* ($p=9.0\times10^{-50}$). Signature 1 therefore appears to reflect changes in gene expression associated with arrest in G1 (O'Leary, Finn and Turner, 2016). When signature 2 was compared to CMAP, the strongest hits were alvocidib and other pan-CDK inhibitors (Figure 1c and Table S2), suggesting that it arises from inhibition of CDKs other than CDK4 and CDK6. To determine the relative magnitude of the G1 arrest and pan-CDK inhibition phenotypes, we scored the absolute mean change in the expression of genes comprising signatures 1 and 2 for each condition. The G1-arrest score was high for all three drugs (Figure S1) whereas the strength of the pan-CDK score varied and was highest for abemaciclib above 0.3 μM and lowest for ribociclib; palbociclib treatment was associated with intermediate scores (Figure 1d).

To better understand the origins of the pan-CDK signature, we collected a substantially larger RNAseq dataset using the high throughput, low-cost RNA sequencing method 3' Digital Gene Expression (DGE-seq) (Soumillon *et al.*, 2014). Seven cell lines, including two that are pRB-deficient (BT-549 and PDX-1258), were exposed for 6 hours to palbociclib, ribociclib, or abemaciclib or to alvocidib (which inhibits CDK1/2/4/6/9); data were collected in triplicate at four CDK4/6 inhibitor

concentrations and two alvocidib concentrations. Differential expression of genes in signatures 1 and 2 (as defined above) was then used to compute G1-arrest and pan-CDK scores for each condition (Figure 2, Table S3). We found that the strength of the average pan-CDK scores was ordered as follows: alvocidib > abemaciclib > palbociclib > ribociclib (Figure 2, x-axis). The pan-CDK signature was also strongly dose-dependent for abemaciclib ($r=0.78$, $p=9.3\times10^{-7}$) and alvocidib ($r=0.76$, $p=1.5\times10^{-3}$). Notably, the score for 0.1 μM and 1 μM alvocidib across all cell lines (green) substantially overlapped abemaciclib at 1 μM and 3 μM (red). G1 arrest scores were dose-dependent for all drugs and substantially higher in pRB-competent than in pRb-deficient cell lines (0.73 vs. 0.25). In the case of ribociclib, only four genes belonging to the G1 signature were differentially regulated in pRB-deficient lines (two-sided Fisher exact test $p=2\times10^{-4}$ as compared to pRB-proficient lines) consistent with the hypothesis that a pure CDK4/6 inhibitor should be inactive in cells lacking pRB, the primary substrate of CDK4/6 kinases. In the case of alvocidib, abemaciclib and palbociclib a non-zero G1 signature most likely arises in pRB-deficient cells because pan-CDK and G1 arrest signatures are not orthogonal and the inhibition of CDKs other than CDK4/6 makes a contribution. However, the converse is not true: a high G1-arrest score can be associated with a pan-CDK score near zero. Taken together, the transcript profiling data strongly suggest that palbociclib, ribociclib, and abemaciclib have different target spectra in breast cancer cells with abemaciclib, and to a lesser extent palbociclib, having features in common with alvocidib. Like alvocidib, abemaciclib is biologically active in pRB-deficient cells, which also demonstrates CDK4/6-independent activities.

Effects of CDK4/6 inhibitors on the activity of CDK/cyclin complexes

To study the effects of CDK4/6 inhibitors on the phosphoproteome we performed isobaric (TMT) tag based liquid-chromatography mass spectrometry (LC/MS) (McAlister *et al.*, 2012). MCF7 cells were treated with DMSO, palbociclib, or abemaciclib for one hour (to focus on immediate-early changes in the phosphoproteome) and a total of 9958 phosphopeptides were detected across all samples;

among these 739 were down-regulated in the presence of palbociclib and 2287 in the presence of abemaciclib (log2 fold-change > 1.5; Figure 3a, Table S4). Enrichment analysis (Drake *et al.*, 2012) involving known kinase-substrate relationships (see Methods) was used to identify kinases whose down-regulation was most likely to account for observed phosphoproteome changes. This analysis showed that inferred activities for CDK4, CDK6, and Aurora A/B kinases (AURKA/B) were significantly down-regulated in both palbociclib and abemaciclib-treated cells and CDK1, CDK2, CaM-kinase II subunit alpha (CAMK2α), TTK, and polo-like kinase 1 (PLK1) were downregulated only in the presence of abemaciclib (Figure 3b, Table S5). Thus, phosphoproteome profiling confirms that abemaciclib has a greater effect on the activity of the kinome than palbociclib and that inhibition of CDKs other than CDK4 and CDK6 is likely involved.

Inference of kinase activity from phosphoproteome data yields both direct and indirect drug targets. We therefore performed three different *in vitro* assays to identify direct targets. KINOMEscan, available as a service from DiscoverX, involves an affinity binding assay between members of a 468 DNA-tagged recombinant kinase library and an immobilized ATP-like ligand; the assay is performed in the presence and absence of an ATP-competitive drug (Fabian *et al.*, 2005). KINOMEscan profiling showed that ribociclib is the most selective CDK4/6 inhibitor and abemaciclib the least (Figure 3c, Figure S2a-b and Table S6); similar data are found in (Gelbert *et al.*, 2014; Chen, N. V Lee, *et al.*, 2016).

Since several CDKs are not found in the KINOMEscan library (e.g. CDK1, CDK6) or are not complexed with cyclins (e.g. CDK2), we also used multiplexed inhibitor bead mass spectrometry (MIB/MS) (Duncan *et al.*, 2012) to obtain kinome profiles. In this assay, a cell lysate is mixed with beads conjugated to pan-kinase inhibitors in the presence and absence of a test drug and the levels of bound kinases then determined by mass spectrometry (Figure 3d, Table S7); to generate a lysate with the greatest number of expressed kinases we mixed several cell types (Médard *et al.*, 2015). We detected 164 kinases, including 13 CDKs in the unfractionated extract by TMT LC/MS, and found that ribociclib,

palbociclib, and abemaciclib all bound to CDK4 and CDK6. In addition, abemaciclib bound to CDK1, CDK2, CDK7 and CDK9; for abemaciclib we also observed strong binding to GSK3α/β and CAMK2γ/δ. These results agreed well with data for abemaciclib recently published by Cousins et al (Spearman's $\rho = 0.62$, $P = 8.9\times10^{-16}$) (Cousins *et al.*, 2017). Moreover, when KINOMEscan data (obtained in the presence of 1 μM abemaciclib) and MIB data (obtained with 10 μM abemaciclib) were compared, 19 of 25 kinases strongly inhibited in the KINOMEscan and also found in cell extracts were significantly reduced in binding to MIBs (log2 fold change > 1.5), demonstrating good reproducibility between different types of assays. We conclude that ribociclib is the most selective CDK4/6 inhibitor tested and abemaciclib the least, with a dose-dependent increase in the number of targets significantly inhibited by abemaciclib from 4 at 0.1 μM drug to 13 at 1 μM and 28 at 10 μM.

To quantify drug effects on individual kinases, we performed in vitro activity assays (SelectScreen assays by Thermo Fisher or HotSpot assays by Reaction Biology; see Methods) at 10 drug concentrations using recombinant human kinases and kinase-cyclin complexes identified as potential targets by transcriptional, phospho-proteomic or kinase profiling assays. The data showed that abemaciclib was the most potent inhibitor of CDK4 and CDK6 and confirmed activity against multiple kinases that were not inhibited, or were only weakly inhibited, by palbociclib or ribociclib (Figure 3e, Figure S3a and Table S8). These kinases include CDK2/cyclin A/E, CDK1/cyclin B, CDK7/cyclin H, CDK9/cyclin K/T1, GSK-3β, CAMK2A, and TTK (Figure S3b). In comparison to the first-generation CDK inhibitor alvocidib, abemaciclib is similar in its activity against CDK2/cyclin A/E and about 10-fold less active against CDK1/cyclin B, CDK7/cyclin H, and CDK9/cyclin K/T1 (potentially explaining the improved toxicity profile of abemaciclib relative to pan-CDK inhibitors), whereas ribociclib and palbociclib were at least one order of magnitude less potent against these kinases. The potency of the three drugs against CDK4 vs. CDK6 was dependent on the cyclin partner and the assay, but the kinases generally differed by no more than 3-fold (Table S8). Results from KINOMEscan, kinobead, and SelectScreen assays were generally concordant with mRNA-seq and phosphoproteome profiling with

three notable exceptions: CDK1 and CDK6 are absent from the KINOMEscan panel and CDK2, while present, does not appear to be active, perhaps because CDK2/cyclin complexes do not form (Echalier *et al.*, 2014). Thus, the widely used KINOMEscan assay misses the ability of abemaciclib to inhibit CDK2-cyclin A/E complexes, an activity that is potentially significant given the ability of these complexes to rescue CDK4/6 inhibition.

Comparing CDK4/6 inhibitors in breast cancer cell lines

To compare the biological activities of CDK4/6 inhibitors, we acquired dose-response curves in 34 breast cancer cell lines spanning all clinical subtypes and computed GR values (Figure 4a and Table S9), which distinguish between drug-induced cell cycle arrest and cell death while correcting for apparent differences in drug sensitivity arising from variable proliferation rates (Hafner *et al.*, 2016; Hafner, Niepel and Sorger, 2017). Both palbociclib and abemaciclib elicited cytostatic responses with GR_{50} values in the 10-100 nM range (Table S10). Potency was highly correlated among the drugs (Spearman's $\rho = 0.91$, $P = 5.7\times10^{-14}$) with abemaciclib ~5.5-fold more potent on average in inducing cytostasis (t-test $P = 5.3\times10^{-7}$); this difference is consistent with a 3-fold difference between palbociclib and abemaciclib in *in vitro* IC_{50} values for CDK4/6 inhibition (as measured *in vitro* by SelectScreen assays; Figure 3e). Efficacy measured by GR values at 0.1 μM varied between 0 (complete cytostasis) and 0.76 (weak growth inhibition) depending on the cell line and was similar for palbociclib and abemaciclib, showing that at these concentrations the drugs only fractionally inhibit cell proliferation. In pRb-deficient cell lines, palbociclib was inactive and abemaciclib had little or no effect below 0.3 μM (yellow lines Figure 4a); thus, the cytostatic response is likely to be a result of CDK4/6 inhibition.

However, abemaciclib also elicited a second response at doses greater than 0.3 μM; this response was characterized by negative GR values and cell death (see Methods; Figure 4a). As a result, the complete dose-response behavior of abemaciclib was significantly better fitted in most cell lines by the product of two sigmoidal curves (Figure 4b, Figure S4, and Methods). The mid-point of the second

response curve was offset to a similar degree as *in vitro* dose-response curves for CDK1/2 vs. CDK4/6 inhibition (Table S8). This behavior is consistent with inhibition of two sets of targets: CDK4/6 at low dose – resulting in G1 arrest – and kinases such as CDK1/2 above 0.3 μM – resulting in cell death. The high-dose drop in GR values was not observed in palbociclib-treated cells nor in the eight cell lines in which GR data were collected for ribociclib. As a result, abemaciclib was substantially more efficacious than palbociclib in inhibiting and killing pRb-proficient cells of all subtypes, having a GR_{max} value on average 0.52 below that of palbociclib (t-test P=4.5×10^{-9}; Table S10).

When we searched a set of 30 cell cycle regulators for those whose mRNA expression levels could discriminate between responsiveness to palbociclib and abemaciclib in pRb-proficient cell lines, and potentially explain variability in abemaciclib-mediated cytotoxicity, we found that a combination of elevated expression of CDKN1A (p21 – an inhibitor of CDK1/2/4/6), CDKL5 (a cyclin-dependent kinase targeted by abemaciclib and other pan-CDK inhibitors based on KINOMEscan data), CCNE1 (cyclin E1, which has been implicated in palbociclib resistance (Sherr, Beach and Shapiro, 2016)) and reduced expression of CDK9 (another abemaciclib and pan-CDK inhibitor target) comprised a strong preclinical pharmacogenomic predictor across the 26 cell lines tested (q^2 = 0.85, P = 2.9×10^{-6} by leave-one-out cross validation; Figure 4c-d).

Abemaciclib blocks cells in the G2 phase of the cell cycle

Consistent with the known biology of CDK4/6 inhibition, abemaciclib, ribociclib, and palbociclib all suppressed pRb phosphorylation and arrested cells in G1 (Figure 5a). The 3-fold difference in drug concentration needed to induce arrest matched measured differences in potency in biochemical assays (with abemaciclib the most potent and ribociclib the least; Figure 3e). A fraction of cells treated with abemaciclib also arrested in G2 rather than G1, particularly at drug concentrations of 0.3 μM and above (Figure 5a, Figure S5a), a possible consequence of inhibition of CDK1 and CDK2, whose activities are required for progression through mitosis and S-phase. Treating pRb-deficient cells

with ribociclib or palbociclib had no effect on proliferation whereas treatment with abemaciclib caused cells to accumulate in G2, consistent with an abemaciclib-induced cell cycle arrest independent of CDK4/6 (Fig. 5b, Fig. S5a-b).

When we compare the scores for G1-arrest and pan-CDK signatures across a range of doses in multiple cell lines we found that pan-CDK score was significant for abemaciclib only above 0.3 μM (P=2.1×10^{-4}, ranksum test); activity was observed in pRB-deficient cells only at concentrations of 1 μM and above. When a drug inhibits multiple targets with different potencies, as observed for abemaciclib, the question arises whether both primary and secondary targets can be engaged at doses achievable *in vivo*. The maximum serum concentration in humans (C_{max}) for abemaciclib is estimated to be 0.5 μM to 1 μM when active metabolites are included (Burke *et al.*, 2016; Patnaik, Lee S. Rosen, *et al.*, 2016) suggesting abemaciclib could have activities such as induction of cell death and G2 arrest at concentrations relevant to clinical use.

Assaying abemaciclib polypharmacology in xenograft tumors

To directly test the hypothesis that abemaciclib is active against kinases other than CDK4/6 in vivo, we generated MCF-7 xenografts in nude mice and exposed them to CDK4/6 inhibitors at a range of doses. When tumors reached ~300 mm^3, animals were randomly assigned to treatment groups and treated daily for 4 days to a vehicle-only control or to 150 mg/kg ribociclib, 150 mg/kg palbociclib or 25-150 mg/kg abemaciclib, doses previously shown to be effective in xenografts (Fry *et al.*, 2004; Gelbert *et al.*, 2014; O'Brien *et al.*, 2014). Animals were euthanized and tumors divided into two samples; one was fixed in formaldehyde and paraffin embedded and the other processed for mRNA-sequencing. FFPE specimens were imaged by immunofluorescence using vimentin and E-cadherin staining to distinguish tumor cells from mouse stroma. We found that all conditions tested resulted in a significant reduction in the fraction of p-pRb positive cells (Dunnett's multiple comparison $P < 0.0001$) providing pharmacodynamic evidence that all tumors were exposed to drug at active concentrations

(Figure 6a). mRNA-seq data showed that all three drugs induced a G1-arrest signature (Figure 6b, Table S11), the strength of which was correlated with the degree of p-pRb inhibition (Spearman's $\rho = -0.80$, $P = 1.1\times10^{-10}$). Furthermore, at doses above 100 mg/kg, abemaciclib (but not ribociclib or palbociclib) also induced a strong pan-CDK signature (Figure 6b). These data provide *in vivo* confirmation that abemaciclib can engage targets other than CDK4 and CDK6, recapitulating the drug's off-target activity in cell culture.

Abemaciclib prevents adaptive response in contrast to palbociclib and ribociclib

As previously described (Herrera-Abreu *et al.*, 2016; Asghar *et al.*, 2017), cells adapt to CDK4/6 inhibition over time. Within 48 hours of exposure to palbociclib or ribociclib we found that cells re-entered the cell cycle and acquired a p-pRb positive state at drug concentrations as high as 3.16 μM (Figure 5a). In contrast, pRb phosphorylation remained low in cells exposed to 1 μM abemaciclib and above (Figure 5a) with ongoing cell death and no evidence of adaptation five days after drug exposure (Figure 7a, Figure S6 and Table S12). In studies designed to assess long-term adaptation to drug, we observed that breast cancer cells grown for several months in the presence of 1 μM palbociclib had higher cyclin E (CCNE1) and lower pRb levels than parental cells (Figure 7b). These palbociclib-adapted cells were cross-resistant to ribociclib (Figure 7c, Figure S7a-b and Table S13) but sensitive to abemaciclib at doses of 1 μM and above, consistent with the ability of abemaciclib to target kinases not inhibited by palbociclib.

We also established a cell line from a patient with advanced/metastatic $HR^{+}/Her2^{-}$ breast cancer whose disease had progressed following eight months on ribociclib/letrozole. The tumor lacked pRb by immunohistochemistry (Figure 7c) as did the derived cell line (MGH312; Figure S7d). These tumor cells were responsive to abemaciclib as judged by inhibition of cell proliferation and induction of cell death but were completely resistant to palbociclib or ribociclib even at high doses (Figure 7d and Table S14). It will remain unknown, however, whether or not this patient (now deceased) could have benefited

from treatment with abemaciclib. Nonetheless, we propose that abemaciclib may have clinically useful activities in a subset of tumors that are not responsive, or have become resistant to, more selective CDK4/6 inhibitors.

DISCUSSION

It is not uncommon for multiple therapeutics targeting the same proteins to be approved in close succession. In the case of CDK4/6 inhibitors, palbociclib, ribociclib and abemaciclib have all proven to be highly effective in the treatment of HR^+ metastatic breast cancer and are currently being tested in ~100 ongoing clinical trials for activity in other malignancies. It has hitherto been assumed that the mechanisms of action of the three approved drugs are very similar, and distinct from those of older-generation CDK inhibitors such as alvocidib: observed differences in the efficacy and toxicity of palbociclib, ribociclib and abemaciclib have been attributed to differences in dosing schedules or potency against CDK4 versus CDK6 (Sherr, Beach and Shapiro, 2016). However, the current paper presents six lines of evidence that ribociclib, palbociclib, abemaciclib and alvocidib actually span a spectrum of selectivity for CDK-cyclin complexes. In particular, Abemaciclib has biochemical and physiological activities not manifest by ribociclib and only weakly by palbociclib. First, exposure of breast cancer cells of different subtypes to CDK4/6 inhibitors induces transcriptional changes associated with G1 arrest and in the case of abemaciclib alone, to dose-dependent transcriptional changes similar to those elicited by alvocidib and arising from pan-CDK inhibition. Second, exposing cells to abemaciclib results in more extensive changes in the phosphoproteome than exposure to palbociclib and kinase inference suggests that this is due in part to inhibition of CDK1 and CDK2. Third, kinome profiling using industry-standard KINOMEscan panels, multiplexed inhibitor bead mass spectrometry, and kinase activity assays confirms that abemaciclib has multiple targets in addition to CDK4/6. Fourth, abemaciclib causes arrest of cells in both the G1 and G2 phases of the cell cycle and the drug is cytotoxic even in the absence of pRb; in contrast, cells exposed to palbociclib and ribociclib arrest only

in G1 and elicit little or no cell death. Fifth, in a mouse xenograft model, abemaciclib induces both CDK4/6-like G1 arrest and pan-CDK transcriptional signatures, as observed in cultured cells. Sixth, whereas abemaciclib durably inhibits cell division, cultured cells adapt within 2-3 days of continuous exposure to palbociclib or ribociclib and resume proliferation. Moreover, a cell line derived from a patient with $HR^{+}/Her2^{-}$ breast cancer that progressed on ribociclib/letrozole remained sensitive to abemaciclib.

Evidence of substantial differences among CDK4/6 inhibitors is scattered throughout the literature but has not been consolidated or rigorously evaluated, consistent with a general lack of comparative biochemical data on many FDA-approved drugs. Large-scale kinase profiling studies using KINOMEscan or MIB/MS are one exception to this generalization (Fabian *et al.*, 2005; Gelbert *et al.*, 2014; Cousins *et al.*, 2017; Klaeger *et al.*, 2017). However, our findings strongly argue for a multi-faceted approach to comparative mechanism of action studies. Proteomic, transcriptional, biochemical, and phenotypic assays measure different aspects of drug action and in the current work a combination of methods was needed to obtain a complete picture of target spectrum. For example, the false negative finding in KINOMEscan data that abemaciclib does not interact with CDK2 may explain why biological differences among CDK4/6 inhibitors have not been widely appreciated. Similarly, whereas GSK3β was found to be an abemaciclib target of borderline significance by phospho-proteome profiling, perhaps reflecting the challenges of inferring changes in kinase activity from data that are inherently under-sampled (Riley and Coon, 2016), it was clearly a target by kinase activity assays (Cousins *et al.*, 2017). Conversely, mRNA and proteomic profiling assays showed that exposure of breast cancer cells to abemaciclib results in inhibition of CDK9, AURKA/B, CAMK2α, TTK, and PLK1 but biochemical experiments showed that AURKA/B and PLK1 are most likely indirect targets of abemaciclib whose activity is downregulated as a secondary consequence of G2 cell cycle arrest (the other kinases appear to be direct targets of abemaciclib). Consistent with Cousins et al. (Cousins *et al.*, 2017), our results using multiple different assays provide little support for the assertion that ribociclib, palbociclib or

abemaciclib are systematically more active against CDK4 than CDK6. Instead, the opposite appears to be true: enzymatic assays show the IC_{50} for CDK4 is about 2.5-fold greater than for CDK6 for all three drugs. Thus, despite frequent assertions that difference in the CDK4/6 ratio among the three drugs might therapeutically significant (Gelbert *et al.*, 2014; Patnaik, Lee S. Rosen, *et al.*, 2016; Patnaik, Lee. S Rosen, *et al.*, 2016) our data suggest that this is unlikely. Both targets are likely to be highly inhibited at therapeutic doses

In the case of a poly-selective drug such as abemaciclib the question arises whether activities observed at different drug concentrations are all biologically relevant. There is no question that CDK4 and CDK6 are the highest affinity targets of abemaciclib and that abemaciclib is the most potent of the three approved drugs against these CDKs. Abemaciclib is 10- to 100-fold less potent against CDK2 and CDK1 than CDK4/6, but we detect the cellular consequences of CDK1/2 inhibition in cell lines at concentrations as low as 0.3 μM, well within the C_{max} range in humans, and also achievable in xenograft mouse models (Raub *et al.*, 2015; Burke *et al.*, 2016; Patnaik, Lee S. Rosen, *et al.*, 2016). Abemaciclib also exhibits substantially reduced drug adaptation with respect to anti-proliferative effects, which is beneficial for an anti-cancer drug.

The current generation of CDK4/6 inhibitors has benefited from a considerable investment in increasing target selectivity, mainly as a means of reducing toxicity relative to earlier generation drugs (Toogood *et al.*, 2005; Asghar *et al.*, 2015; Peplow, 2017). However, our results suggest that the activities of abemaciclib against kinases other than CDK4/6 are beneficial for anti-cancer activity and targeting them jointly with CDK4/6 may be a means to achieve more durable responses than with CDK4/6 inhibition alone. In particular, blocking CDK2/cyclin E should mitigate resistance resulting from amplification of cyclin E (Dean *et al.*, 2010; Herrera-Abreu *et al.*, 2016) and also achieve a more complete therapeutic response by targeting mitotic cells with high CDK2 activity (Asghar *et al.*, 2017) – a strategy explicitly being tested by Pfizer through clinical development of a CDK2/4/6 inhibitor (US patent 20180044344A1). Inhibition of CDK1/7/9 may also contribute to cell killing (Kitada *et al.*, 2000;

Wittmann *et al.*, 2003) and inhibition of mitotic kinases such as TTK may enhance tumor immunogenicity, a key contributor to drug response (Luen *et al.*, 2016).

Clinical implications

Our findings show that abemaciclib is not equivalent to palbociclib or ribociclib in a preclinical setting and they provide a rationale for treating patients with abemaciclib following disease progression on palbociclib or ribociclib: cells, including cells derived from a patient, that have become resistant to these two drugs remain sensitive to abemaciclib. Using breast cancer cell lines, we identified a simple pharmacogenomics signature predicting the incremental efficacy of abemaciclib relative to palbociclib; this signature includes genes (*CDKN1A, CDKL5, CCNE1* and *CDK9*) with a clear biological connection to CDK inhibition and suggests the possibility of developing predictive signatures relevant to drug selection in human patients. The enhanced activities of abemaciclib relative to other CDK4/6 inhibitors are observed at concentrations of 0.3 μM and above, overlapping human C_{max} concentrations. However, further studies are needed to determine how *in vitro* efficacy translates to patients and if incremental benefit from treatment with abemaciclib is observed. This is particularly true in the case of pRb-deficient tumors, in which abemaciclib's efficacy relies on micromolar concentrations. An alternative is to combine CDK4/6 inhibitors with drugs that inhibit abemaciclib's secondary targets or develop molecules that jointly inhibit CDK4/6 and CDK2, a strategy Pfizer is pursuing. In all of these cases, our work shows that polypharmacology can be exploited to achieve more durable responses than with "pure" CDK4/6 inhibitors such as ribociclib.

Acknowledgements. This work was funded by P50-GM107618, U54-CA225088 and U54-HL127365 to PKS and DJ. We thank LSP member M. Berberich for skilled assistance, the ICCB for help with

automation, S. Gygi for use of software and computing facilities for proteomics, and A. Bardia for comments.

Author contributions. MH, CEM, and DJ conceived the study; MH, CEM, DJ, and PKS designed the experiments and CEM, MC, SAB, and RAE performed them. MH, KS, and CC performed the computational analyses. CSW and DJ obtained the patient-derived line and provided related data. PKS oversaw the experimental and computational research; MH, CEM, KS, DJ, and PKS wrote the manuscript.

FIGURE LEGENDS

Figure 1: Transcriptional responses of breast cancer cell lines to CDK4/6 inhibitors. (a) Clustering of transcriptional response for seven breast cancer cell lines treated for 6 or 24 hours with ribociclib, palbociclib, or abemaciclib at 0.3, 1, or 3 μM. Only genes for which statistically significant (FDR < 0.2) changes were observed in at least 3 conditions are shown. Down-regulated genes comprising signature 1 and 2 are outlined in red and cyan, respectively. **(b-c)** Enrichment scores for signature 1 (b) and 2 (c) based on L1000 signatures identified by Enrichr (see Methods). **(d)** Score of the pan-CDK transcriptional signature per cell line following six hours of exposure to drug based on the RNA-seq data from panel (a).

Figure 2: G1-arrest and pan-CDK scores induced by CDK4/6 inhibitors. Score of the G1-arrest signature relative to the pan-CDK signature for seven cell lines treated with palbociclib, ribociclib, abemaciclib or alvociclib at 0.1, 0.3, 1, or 3 μM; squares denote pRb-deficient lines. Distributions of scores for pRb-competent lines at are shown at the margins for each signature.

Figure 3: inhibition of CDK/cyclin activity by CDK4/6 inhibitors. (a) Clustering of changes in phosphopeptide levels for MCF7 cells treated for 1 hour with either abemaciclib or palbociclib at 0.3 or 3 μM. **(b)** Normalized enrichment scores for kinases based on the phosphoproteomic data in panel (a). Only kinases inferred as down-regulated in at least two conditions are displayed; drugs and concentrations at which differences are significant (FDR < 0.2) are shaded. **(c)** Inhibition of the top 100 inhibited kinases plus CDK2, and AURKA at 0.1 and 1 μM of each CDK4/6 inhibitor measured by the KINOMEscan assay (see Figure S2). **(d)** The degree of inhibition (log2 fold change) of each CDK detected by MIB/MS after treating a mixed cell lysate with a CDK4/6 inhibitor at the doses indicated. **(e)** *In vitro* kinase activity assays confirm inhibition of additional targets by abemaciclib. Comparison of

IC_{50} values for CDK4/6 inhibitors and alvocidib as measured using purified kinases and 10-point *in vitro* dose-response assays (see Figure S3).

Figure 4: Comparison of the phenotypic response of breast cancer cell lines to CDK4/6 inhibitors. **(a)** GR curves for cell growth (top) and increased percent of dead cells over vehicle-only control conditions (bottom) for 26 pRb-proficient breast cancer cell lines (blue) and 8 pRb-deficient cell lines (yellow) treated with palbociclib (left) or abemaciclib (right) for 72 hours. The vertical box illustrates the maximum serum concentration for abemaciclib (C_{max}). **(b)** Dose-response curve for palbociclib (red) and abemaciclib (blue) in MCF7 cells. Dotted lines depict two fitted sigmoidal curves whose product optimally recapitulates the blue curve with extracted values for GEC_{50} (50%-maximal effective concentration) shown below and for GR_{max} (maximal efficacy) shown to the right (See Figure S4). **(c)** Performance of a pharmacogenomics predictor of palbociclib vs. abemaciclib drug response based on mRNA levels for 30 cell cycle regulators; plots shows the observed versus predicted (leave-one-out cross validation) difference in GR value at 3 μM between palbociclib and abemaciclib based on a linear model of **(d)** The predictor coefficients from the model in (c), error bars represent the standard error of the model.

Figure 5: Comparison of the effects of ribociclib, palbociclib, and abemaciclib on the cell cycle. (a) Distribution of DNA content in MCF7 cells exposed to one of three CDK4/6 inhibitors over a range of concentrations for 24 (left) or 48 (right) hours. In each curve the phospho-pRb positive cell population is depicted in a darker shade. One representative replicate out of three is shown. **(b)** Distribution of DNA content for PDX12-58 cells, which are pRb-deficient, exposed to abemaciclib for 48 hours at a range of concentrations (see Figure S6 for palbociclib and ribociclib results). These data represent one of three biological replicates.

Figure 6: Transcriptional response of MCF-7 xenografted cells to CDK4/6 inhibitors

(a) Fraction of phospho-pRb positive tumor cells in MCF-7 xenografts after four days of drug treatment. **(b)** Score of the pan-CDK transcriptional signature as compared to the G1-arrest signature across MCF-7 tumors following four days of exposure to drug; same analysis as in Figure 2.

Figure 7: Acute and adaptive responses of breast cancer cell lines and tumors to CDK4/6 inhibitors. (a) Time-dependent GR values for MCF7, Hs 578T, and PDX12-58 cells treated with 3.16 μM ribociclib, palbociclib, or abemaciclib for five days (increased percent of dead cells over vehicle-only control conditions shown in Figure S6). One representative replicate out of four is shown. **(b)** Western Blots of cyclin E and total pRb levels in Hs 578T and MCF7 parental cells and cells adapted to grow in 1 μM palbociclib. **(c)** GR values for Hs 578T and MCF7 parental cells and cells adapted to grow in 1 μM palbociclib in response to treatment with 3.16 μM ribociclib, palbociclib, or abemaciclib for 72 h (see Figure S7). * denotes $P < 0.05$; ** denotes $P < 0.01$ as measured using a t-test with six replicates in each group. Error bars denote SEM of six replicates. **(d)** GR values (left) and increased percent of dead cells over vehicle-only control conditions (right) for the patient-derived line MGH312 in response to 96-hour treatments with ribociclib, palbociclib, or abemaciclib. Error bars show the SEM of three replicates.

SUPPLEMENTAL FIGURE LEGENDS

Figure S1, Related to Figure 1: G1-arrest transcriptional signature score. Score of the G1-arrest transcriptional signature per cell line following 6 hours of exposure to drug based on the RNA-seq data from Fig 1a.

Figure S2, Related to Figure 3: KINOMEscan results for the three CDK4/6 inhibitors. (a) Kinases with less than 10% activity remaining for drug concentrations of 0.1 μM and 1.0 μM of each of the three CDK4/6 inhibitors (see Table S6). Images generated using the TREEspotTM Software Tool and reprinted with permission from KINOMEscan®, a division of DiscoveRx Corporation, © DISCOVERX CORPORATION 2010. **(b)** The differential binding between 0.1 μM and 1.0 μM of the 100 most bound kinases, plus CDK2 and AURKA, for all drugs.

Figure S3, Related to Figure 3: In vitro activity of CDK4/6 inhibitors and alvocidib. (a) Unbound fraction or inhibition curves for select kinase targets with increasing concentrations of CDK4/6 inhibitors or alvocidib (see Methods for assay details). Error bars are the SEM of two replicates. **(b)** Comparison of IC_{50} values for CDK4/6 inhibitors and alvocidib for select kinases and CDK/cyclin complexes.

Figure S4, Related to Figure 4: Comparison of fit parameters defined in Fig. 4b for the dose response curves for palbociclib and abemaciclib shown in Fig. 4a. (top) Mid-point concentrations for palbociclib (left) and the 2nd phase of abemaciclib (right) versus the mid-point concentrations for the 1st phase of abemaciclib. (bottom) Maximal efficacy for 1st phase of abemaciclib (left) and abemaciclib (right) versus the maximal efficacy of palbociclib.

Figure S5, Related to Figure 5: Effect of CDK4/6 inhibitors on the distribution of cells through the cell cycle. (a) DNA content versus EdU intensity for three breast cancer cell lines either untreated or

treated for 24 hours with 1.0 μM of ribociclib, palbociclib, or abemacicib (from left to right). Color intensity reflects density of cells; numbers represent the percentage of cells in each phase of the cell cycle based on automated gating (blue lines). **(b)** Distribution of DNA content for PDX12-58 cells, which are pRb-deficient, exposed to either ribociclib or palbociclib for 48 hours at a range of concentrations. These data represent one of three biological replicates.

Figure S6, Related to Figure 7: Time dependent increase in the fraction of dead cells treated with CDK4/6 inhibitors. Increased percent of dead cells treated with 3.16 μM ribociclib, palbociclib, or abemaciclib relative to control conditions over time (see Fig. 7a).

Figure S7, Related to Figure 7: Characterization of CDK4/6-inhibitor resistant cell lines. (a) GR values for cell lines adapted to grow in 1 μM palbociclib and their parental lines in response to 72-hour treatments with ribociclib, palbociclib, or abemaciclib. Error bars show the SEM of six replicates. **(b)** Increased percent of dead cells over vehicle-only control conditions for cell lines adapted to grow in 1 μM palbociclib and their parental lines in response to 72-hour treatments with ribociclib, palbociclib, or abemaciclib. Error bars show the SEM of six replicates. **(c)** pRb immunohistochemistry staining of the patient biopsy at the site from which the cell line MGH312 was derived. **(d)** Western Blot of pRb for MCF7, BT-549, and MGH312 cells.

REFERENCES

Asghar, U. *et al.* (2015) 'The history and future of targeting cyclin-dependent kinases in cancer therapy', *Nature Reviews Drug Discovery*. Nature Publishing Group, 14(2), pp. 130–146. doi: 10.1038/nrd4504.

Asghar, U. *et al.* (2017) 'Single-Cell Dynamics Determines Response to CDK4/6 Inhibition in Triple-Negative Breast Cancer.', *Clinical cancer research : an official journal of the American Association for Cancer Research*, 23(18), pp. 5561–5572. doi: 10.1158/1078-0432.CCR-17-0369.

Balko, J. M. *et al.* (2014) 'Molecular profiling of the residual disease of triple-negative breast cancers after neoadjuvant chemotherapy identifies actionable therapeutic targets.', *Cancer discovery*, 4(2), pp. 232–45. doi: 10.1158/2159-8290.CD-13-0286.

Beausoleil, S. A. *et al.* (2006) 'A probability-based approach for high-throughput protein phosphorylation analysis and site localization.', *Nature biotechnology*, 24(10), pp. 1285–92. doi: 10.1038/nbt1240.

Burke, T. *et al.* (2016) 'Abstract 2830: The major human metabolites of abemaciclib are inhibitors of CDK4 and CDK6', *Cancer Research*, 76(14 Supplement), pp. 2830–2830. doi: 10.1158/1538-7445.AM2016-2830.

Caunt, C. J. *et al.* (2015) 'MEK1 and MEK2 inhibitors and cancer therapy: the long and winding road.', *Nature reviews. Cancer*, 15(10), pp. 577–92. doi: 10.1038/nrc4000.

Chen, P., Lee, N. V, *et al.* (2016) 'Spectrum and Degree of CDK Drug Interactions Predicts Clinical Performance', (i), pp. 1–11. doi: 10.1158/1535-7163.MCT-16-0300.

Chen, P., Lee, N. V., *et al.* (2016) 'Spectrum and Degree of CDK Drug Interactions Predicts Clinical Performance.', *Molecular cancer therapeutics*, 15(10), pp. 2273–2281. doi: 10.1158/1535-7163.MCT-16-0300.

Cousins, E. M. *et al.* (2017) 'Competitive Kinase Enrichment Proteomics Reveals that Abemaciclib Inhibits GSK3β and Activates WNT Signaling', *Molecular Cancer Research*. Available at: http://mcr.aacrjournals.org/content/early/2018/01/10/1541-7786.MCR-17-0468.abstract.

Cristofanilli, M. *et al.* (2016) 'Fulvestrant plus palbociclib versus fulvestrant plus placebo for treatment of hormone-receptor-positive, HER2-negative metastatic breast cancer that progressed on previous endocrine therapy (PALOMA-3): final analysis of the multicentre, double-blind, phas', *The Lancet. Oncology*, 17(4), pp. 425–39. doi: 10.1016/S1470-2045(15)00613-0.

Crystal, A. S. *et al.* (2014) 'Patient-derived models of acquired resistance can identify effective drug combinations for cancer', *Science*, 346(6216), p. 1480 LP-1486. Available at: http://science.sciencemag.org/content/346/6216/1480.abstract.

Dean, J. L. *et al.* (2010) 'Therapeutic CDK4/6 inhibition in breast cancer: key mechanisms of response and failure.', *Oncogene*, 29(28), pp. 4018–32. doi: 10.1038/onc.2010.154.

Dickler, M. N. *et al.* (2016) 'MONARCH1: Results from a phase II study of abemaciclib, a CDK4 and CDK6 inhibitor, as monotherapy, in patients with HR+/HER2- breast cancer, after chemotherapy for advanced disease.', *J Clin Oncol 34*, 34.

Drake, J. M. *et al.* (2012) 'Oncogene-specific activation of tyrosine kinase networks during prostate cancer progression', *Proceedings of the National Academy of Sciences*. doi: 10.1073/pnas.1120985109.

Duncan, J. S. *et al.* (2012) 'Dynamic Reprogramming of the Kinome in Response to Targeted MEK Inhibition in Triple-Negative Breast Cancer', *Cell*, 149(2), pp. 307–321. doi: https://doi.org/10.1016/j.cell.2012.02.053.

Echalier, A. *et al.* (2014) 'An inhibitor's-eye view of the atp-binding site of CDKs in different regulatory states', *ACS Chemical Biology*, 9(6), pp. 1251–1256. doi: 10.1021/cb500135f.

Eng, J. K., McCormack, A. L. and Yates, J. R. (1994) 'An approach to correlate tandem mass spectral data of peptides with amino acid sequences in a protein database.', *Journal of the American Society for Mass Spectrometry*, 5(11), pp. 976–89. doi: 10.1016/1044-0305(94)80016-2.

Fabian, M. A. *et al.* (2005) 'A small molecule–kinase interaction map for clinical kinase inhibitors', *Nature Biotechnology*. Nature Publishing Group, 23, p. 329. Available at: http://dx.doi.org/10.1038/nbt1068.

Finn, R. S. *et al.* (2009) 'PD 0332991, a selective cyclin D kinase 4/6 inhibitor, preferentially inhibits proliferation of luminal estrogen receptor-positive human breast cancer cell lines in vitro.', *Breast cancer research : BCR*, 11(5), p. R77. doi: 10.1186/bcr2419.

Franco, J., Witkiewicz, A. K. and Knudsen, E. S. (2014) 'CDK4/6 inhibitors have potent activity in combination with pathway selective therapeutic agents in models of pancreatic cancer', *Oncotarget*, 5(15), pp. 6512–6525. doi: 10.18632/oncotarget.2270.

Fry, D. W. *et al.* (2004) 'Specific inhibition of cyclin-dependent kinase 4/6 by PD 0332991 and associated antitumor activity in human tumor xenografts', *Molecular Cancer Therapeutics*, 3(11), p. 1427 LP-1438. Available at: http://mct.aacrjournals.org/content/3/11/1427.abstract.

Gelbert, L. M. *et al.* (2014) 'Preclinical characterization of the CDK4/6 inhibitor LY2835219: in-vivo cell cycle-dependent/independent anti-tumor activities alone/in combination with gemcitabine.', *Investigational new drugs*, 32(5), pp. 825–37. doi: 10.1007/s10637-014-0120-7.

Goel, S. *et al.* (2016) 'Overcoming Therapeutic Resistance in HER2-Positive Breast Cancers with CDK4/6 Inhibitors.', *Cancer cell*, 29(3), pp. 255–69. doi: 10.1016/j.ccell.2016.02.006.

Griggs, J. J. and Wolff, A. C. (2017) 'Cyclin-Dependent Kinase 4/6 Inhibitors in the Treatment of Breast Cancer: More Breakthroughs and an Embarrassment of Riches.', *Journal of clinical oncology : official journal of the American Society of Clinical Oncology*, p. JCO2017739375. doi: 10.1200/JCO.2017.73.9375.

Hafner, M. *et al.* (2016) 'Growth rate inhibition metrics correct for confounders in measuring sensitivity to cancer drugs', *Nature Methods*, 13(6), pp. 521–527. doi: 10.1038/nmeth.3853.

Hafner, M. *et al.* (2017) 'Designing Drug-Response Experiments and Quantifying their Results', *Current Protocols in Chemical Biology*, 9.

Hafner, M., Niepel, M. and Sorger, P. K. (2017) 'Alternative drug sensitivity metrics improve preclinical cancer pharmacogenomics.', *Nature biotechnology*, 35(6), pp. 500–502. doi: 10.1038/nbt.3882.

Herrera-Abreu, M. T. *et al.* (2016) 'Early Adaptation and Acquired Resistance to CDK4/6 Inhibition in Estrogen Receptor–Positive Breast Cancer', *Cancer Research*, 76(8), pp. 2301–2313. doi: 10.1158/0008-5472.CAN-15-0728.

Horn, H. *et al.* (2014) 'KinomeXplorer: an integrated platform for kinome biology studies.', *Nature methods*, 11(6), pp. 603–4. doi: 10.1038/nmeth.2968.

Hornbeck, P. V. *et al.* (2012) 'PhosphoSitePlus: A comprehensive resource for investigating the structure and function of experimentally determined post-translational modifications in man and mouse', *Nucleic Acids Research*, 40(D1). doi: 10.1093/nar/gkr1122.

Hortobagyi, G. N. *et al.* (2016) 'Ribociclib as First-Line Therapy for HR-Positive, Advanced Breast Cancer', *New England Journal of Medicine*, 375(18), pp. 1738–1748. doi: 10.1056/NEJMoa1609709.

Kettenbach, A. N. and Gerber, S. A. (2011) 'Rapid and Reproducible Single-Stage Phosphopeptide Enrichment of Complex Peptide Mixtures: Application to General and Phosphotyrosine-Specific Phosphoproteomics Experiments', *Analytical Chemistry*, 83(20), pp. 7635–7644. doi: 10.1021/ac201894j.

Kim, S. *et al.* (2013) 'Abstract PR02: LEE011: An orally bioavailable, selective small molecule inhibitor of CDK4/6– Reactivating Rb in cancer.', *Molecular Cancer Therapeutics*, 12(11 Supplement), p. PR02 LP-PR02. Available at: http://mct.aacrjournals.org/content/12/11_Supplement/PR02.abstract.

Kitada, S. *et al.* (2000) 'Protein kinase inhibitors flavopiridol and 7-hydroxy-staurosporine down-regulate antiapoptosis proteins in B-cell chronic lymphocytic leukemia', *Blood*, 96(2), pp. 393–397. Available at: papers2://publication/uuid/D346C111-E276-4328-8AF9-4D06C2B6FB1E.

Klaeger, S. *et al.* (2017) 'The target landscape of clinical kinase drugs', *Science*, 358(6367). Available at: http://science.sciencemag.org/content/358/6367/eaan4368.abstract.

Knudsen, E. S. *et al.* (2017) 'Biological specificity of CDK4/6 inhibitors: dose response relationship, *in vivo* signaling, and composite response signature', *Oncotarget*, 8(27), pp. 43678–43691. doi: 10.18632/oncotarget.18435.

Kuleshov, M. V. *et al.* (2016) 'Enrichr: a comprehensive gene set enrichment analysis web server 2016 update', *Nucleic Acids Research*, 44(W1), pp. W90–W97. doi: 10.1093/nar/gkw377.

Lamb, J. *et al.* (2006) 'The Connectivity Map: using gene-expression signatures to connect small molecules, genes, and disease.', *Science (New York, N.Y.)*, 313(5795), pp. 1929–35. doi: 10.1126/science.1132939.

Lim, J. S. J., Turner, N. C. and Yap, T. A. (2016) 'CDK4/6 Inhibitors: Promising Opportunities beyond Breast Cancer.', *Cancer discovery*, 6(7), pp. 697–9. doi: 10.1158/2159-8290.CD-16-0563.

Lin, J.-R. *et al.* (2017) 'A simple open-source method for highly multiplexed imaging of single cells in tissues and tumours', *bioRxiv*. Available at: http://biorxiv.org/content/early/2017/06/19/151738.abstract.

Luen, S. *et al.* (2016) 'The genomic landscape of breast cancer and its interaction with host immunity', *Breast*, 29, pp. 241–250. doi: 10.1016/j.breast.2016.07.015.

McAlister, G. C. *et al.* (2012) 'Increasing the multiplexing capacity of TMTs using reporter ion

isotopologues with isobaric masses.', *Analytical chemistry*, 84(17), pp. 7469–78. doi: 10.1021/ac301572t.

McAlister, G. C. *et al.* (2014) 'MultiNotch MS3 enables accurate, sensitive, and multiplexed detection of differential expression across cancer cell line proteomes.', *Analytical chemistry*, 86(14), pp. 7150–8. doi: 10.1021/ac502040v.

McCain, J. (2015) 'First-in-Class CDK4/6 Inhibitor Palbociclib Could Usher in a New Wave of Combination Therapies for HR+, HER2- Breast Cancer.', *P & T : a peer-reviewed journal for formulary management*, 40(8), pp. 511–20. Available at: http://www.pubmedcentral.nih.gov/articlerender.fcgi?artid=4517534&tool=pmcentrez&rendertype=abstract.

McCarthy, D. J., Chen, Y. and Smyth, G. K. (2012) 'Differential expression analysis of multifactor RNA-Seq experiments with respect to biological variation', *Nucleic Acids Research*, 40(10), pp. 4288–4297. Available at: http://dx.doi.org/10.1093/nar/gks042.

Médard, G. *et al.* (2015) 'Optimized Chemical Proteomics Assay for Kinase Inhibitor Profiling', *Journal of Proteome Research*. American Chemical Society, 14(3), pp. 1574–1586. doi: 10.1021/pr5012608.

Meloche, S. and Pouysségur, J. (2007) 'The ERK1/2 mitogen-activated protein kinase pathway as a master regulator of the G1- to S-phase transition', *Oncogene*, 26(22), pp. 3227–3239. doi: 10.1038/sj.onc.1210414.

O'Brien, N. *et al.* (2018) 'Preclinical Activity of Abemaciclib Alone or in Combination with Antimitotic and Targeted Therapies in Breast Cancer', *Molecular Cancer Therapeutics*, 17(5), p. 897 LP-907. Available at: http://mct.aacrjournals.org/content/17/5/897.abstract.

O'Leary, B., Finn, R. S. and Turner, N. C. (2016) 'Treating cancer with selective CDK4/6 inhibitors', *Nature Reviews Clinical Oncology*. Nature Publishing Group, 13(7), pp. 417–430. doi: 10.1038/nrclinonc.2016.26.

O'Brien, N. A. *et al.* (2014) 'Abstract 4756: In vivo efficacy of combined targeting of CDK4/6, ER and PI3K signaling in ER+ breast cancer', *Cancer Research*, 74(19 Supplement), p. 4756 LP-4756. Available at: http://cancerres.aacrjournals.org/content/74/19_Supplement/4756.abstract.

Palechor-Ceron, N. *et al.* (2013) 'Radiation Induces Diffusible Feeder Cell Factor(s) That Cooperate with ROCK Inhibitor to Conditionally Reprogram and Immortalize Epithelial Cells', *The American Journal of Pathology*, 183(6), pp. 1862–1870. doi: 10.1016/j.ajpath.2013.08.009.

Patnaik, A., Rosen, L. S., *et al.* (2016) 'Efficacy and Safety of Abemaciclib, an Inhibitor of CDK4 and CDK6, for Patients with Breast Cancer, Non–Small Cell Lung Cancer, and Other Solid Tumors', *Cancer Discovery*, 6(7). Available at: http://cancerdiscovery.aacrjournals.org/content/6/7/740 (Accessed: 2 May 2017).

Patnaik, A., Rosen, L. S., *et al.* (2016) 'Single-Agent Abemaciclib Active in Breast Cancer.', *Cancer discovery*, 6(8), pp. 809–10. doi: 10.1158/2159-8290.CD-NB2016-081.

Paulo, J. A. *et al.* (2015) 'Effects of MEK inhibitors GSK1120212 and PD0325901 in vivo using 10-plex quantitative proteomics and phosphoproteomics.', *Proteomics*, 15(2–3), pp. 462–73. doi:

10.1002/pmic.201400154.

Peplow, M. (2017) 'Astex shapes CDK4/6 inhibitor for approval', *Nature biotechnology*, 35, pp. 395–396.

Rappsilber, J., Mann, M. and Ishihama, Y. (2007) 'Protocol for micro-purification, enrichment, pre-fractionation and storage of peptides for proteomics using StageTips.', *Nature protocols*, 2(8), pp. 1896–906. doi: 10.1038/nprot.2007.261.

Raub, T. J. *et al.* (2015) 'Brain Exposure of Two Selective Dual CDK4 and CDK6 Inhibitors and the Antitumor Activity of CDK4 and CDK6 Inhibition in Combination with Temozolomide in an Intracranial Glioblastoma Xenograft', *Drug Metabolism and Disposition*, 43(9), p. 1360 LP-1371. Available at: http://dmd.aspetjournals.org/content/43/9/1360.abstract.

Reid, Y. *et al.* (2004) *Authentication of Human Cell Lines by STR DNA Profiling Analysis*, *Assay Guidance Manual*. Available at: http://www.ncbi.nlm.nih.gov/pubmed/23805434.

Riley, N. M. and Coon, J. J. (2016) 'Phosphoproteomics in the Age of Rapid and Deep Proteome Profiling', *Analytical Chemistry*, 88(1), pp. 74–94. doi: 10.1021/acs.analchem.5b04123.

Robinson, M. D., McCarthy, D. J. and Smyth, G. K. (2010) 'edgeR: a Bioconductor package for differential expression analysis of digital gene expression data', *Bioinformatics*, 26(1), pp. 139–140. doi: 10.1093/bioinformatics/btp616.

Schwanhäusser, B. *et al.* (2011) 'Global quantification of mammalian gene expression control', *Nature*. Nature Publishing Group, a division of Macmillan Publishers Limited. All Rights Reserved., 473, p. 337. Available at: https://doi.org/10.1038/nature10098.

Sherr, C. J., Beach, D. and Shapiro, G. I. (2016) 'Targeting CDK4 and CDK6: From Discovery to Therapy.', *Cancer discovery*, 6(4), pp. 353–67. doi: 10.1158/2159-8290.CD-15-0894.

Sledge, G. W. *et al.* (2017) 'MONARCH 2: Abemaciclib in Combination With Fulvestrant in Women With HR+/HER2- Advanced Breast Cancer Who Had Progressed While Receiving Endocrine Therapy.', *Journal of clinical oncology : official journal of the American Society of Clinical Oncology*, p. JCO2017737585. doi: 10.1200/JCO.2017.73.7585.

Soumillon, M. *et al.* (2014) 'Characterization of directed differentiation by high-throughput single-cell RNA-Seq', *bioRxiv*. Available at: http://biorxiv.org/content/early/2014/03/05/003236.abstract.

Srivastava, A. *et al.* (2016) 'RapMap: a rapid, sensitive and accurate tool for mapping RNA-seq reads to transcriptomes.', *Bioinformatics (Oxford, England)*. England, 32(12), pp. i192–i200. doi: 10.1093/bioinformatics/btw277.

Subramanian, A. *et al.* (2005) 'Gene set enrichment analysis: A knowledge-based approach for interpreting genome-wide expression profiles', *Proceedings of the National Academy of Sciences*, 102(43), pp. 15545–15550. doi: 10.1073/pnas.0506580102.

Svensson, V. *et al.* (2017) 'Power analysis of single-cell RNA-sequencing experiments', *Nature Methods*. Nature Publishing Group, a division of Macmillan Publishers Limited. All Rights Reserved., 14, p. 381. Available at: http://dx.doi.org/10.1038/nmeth.4220.

Ting, L. *et al.* (2011) 'MS3 eliminates ratio distortion in isobaric multiplexed quantitative proteomics.', *Nature methods*, 8(11), pp. 937–40. doi: 10.1038/nmeth.1714.

Toogood, P. L. *et al.* (2005) 'Discovery of a potent and selective inhibitor of cyclin-dependent kinase 4/6', *Journal of Medicinal Chemistry*, 48(7), pp. 2388–2406. doi: 10.1021/jm049354h.

Torres-guzmán, R. *et al.* (2017) 'Preclinical characterization of abemaciclib in hormone receptor positive breast cancer'.

Wittmann, S. *et al.* (2003) 'Flavopiridol down-regulates antiapoptotic proteins and sensitizes human breast cancer cells to epothilone B-induced apoptosis', *Cancer Research*, 63(1), pp. 93–99.

Yang, C. *et al.* (2017) 'Acquired CDK6 amplification promotes breast cancer resistance to CDK4/6 inhibitors and loss of ER signaling and dependence', *Oncogene*, 36(16), pp. 2255–2264. doi: 10.1038/onc.2016.379.

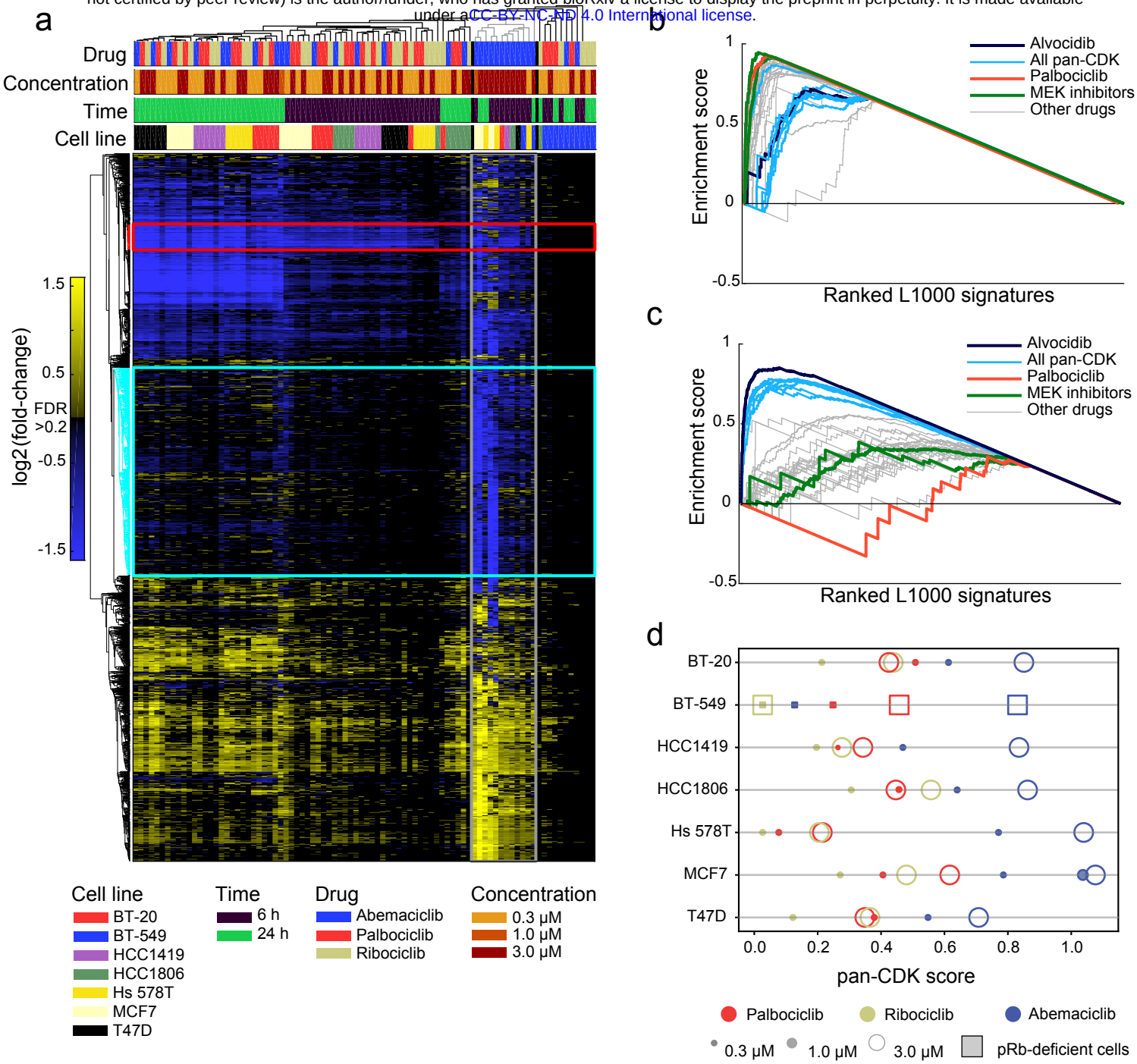

Figure 1

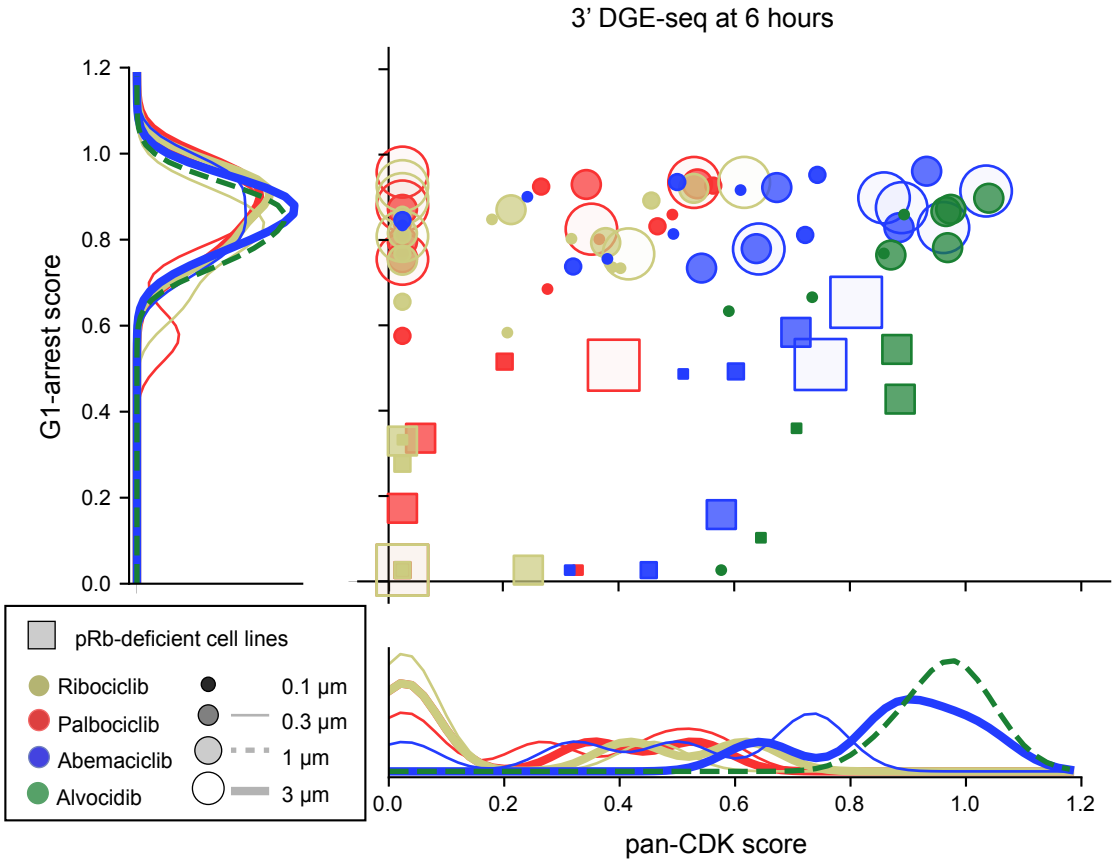

Figure 2

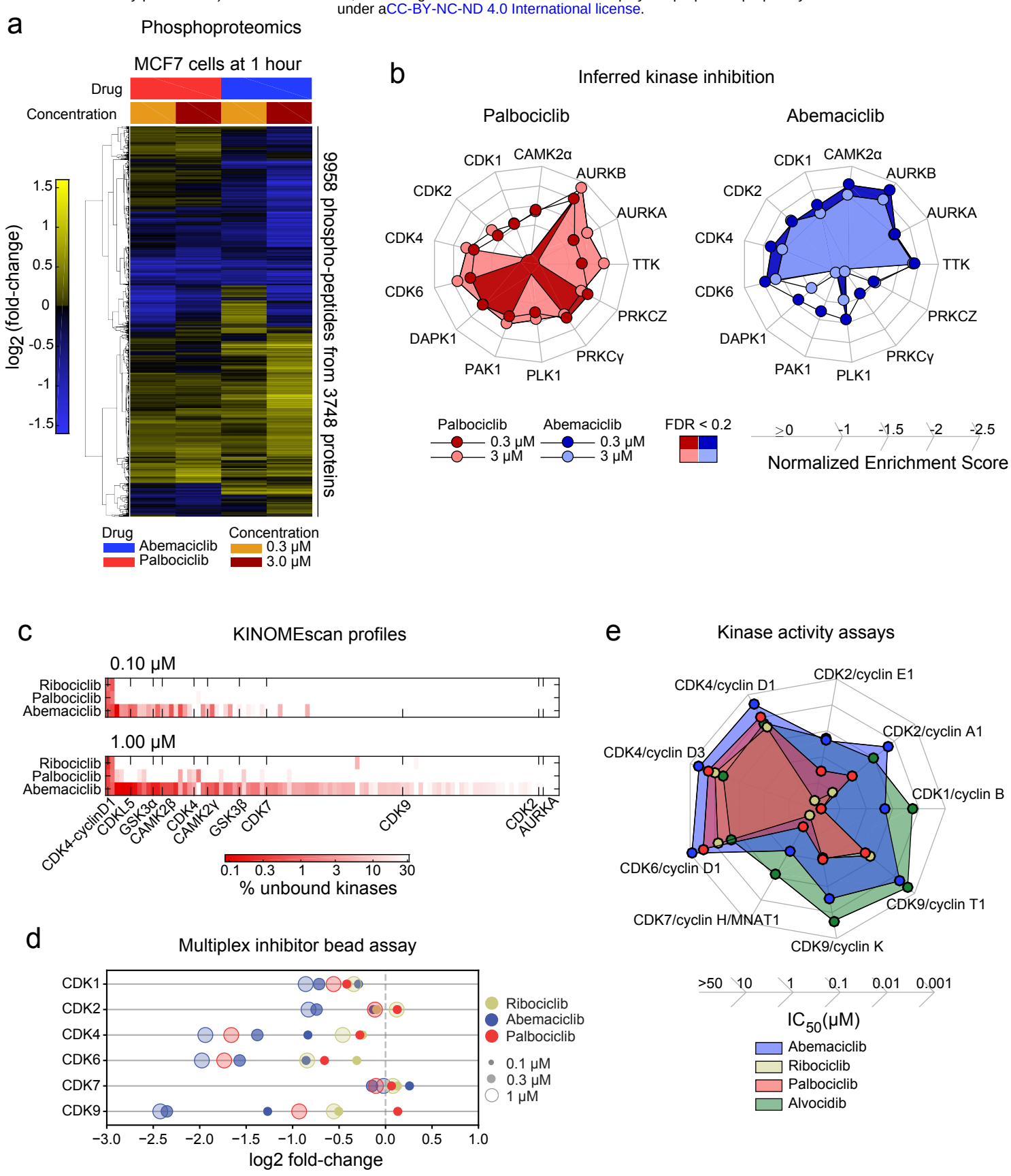

Figure 3

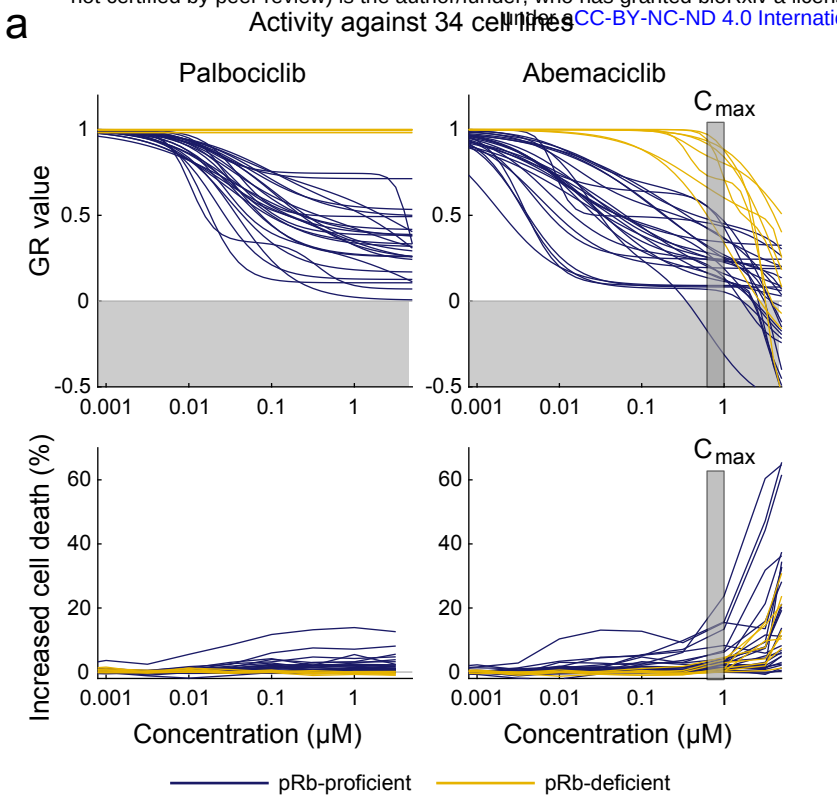

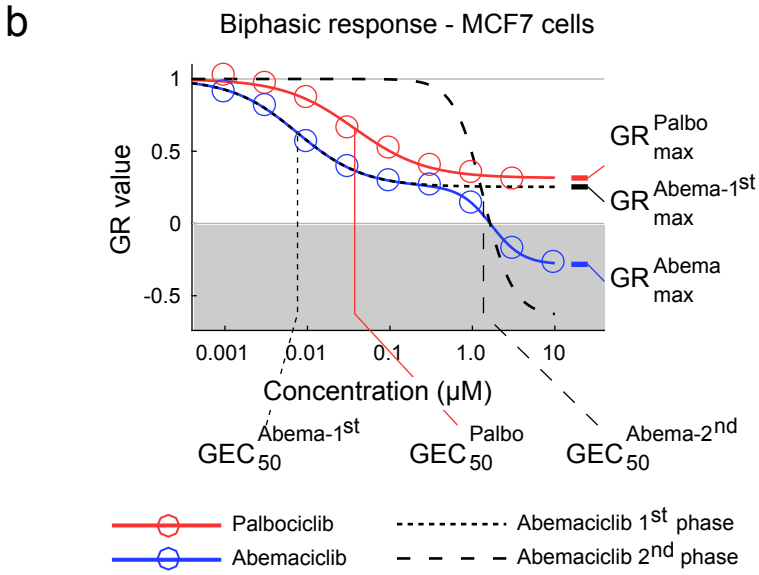

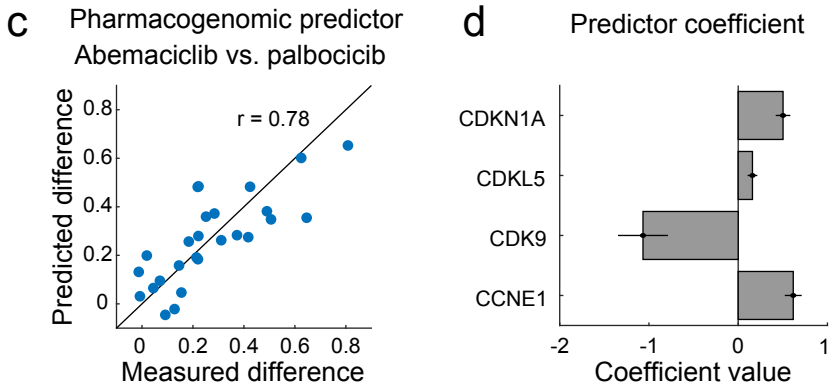

Figure 4

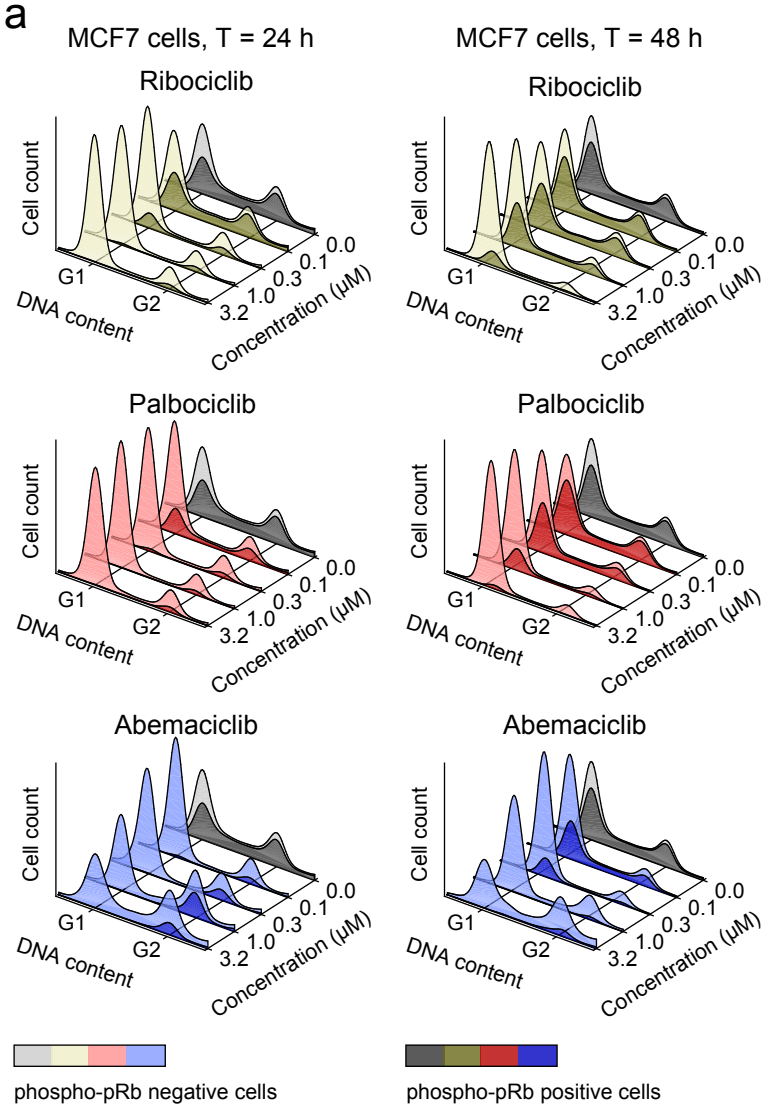

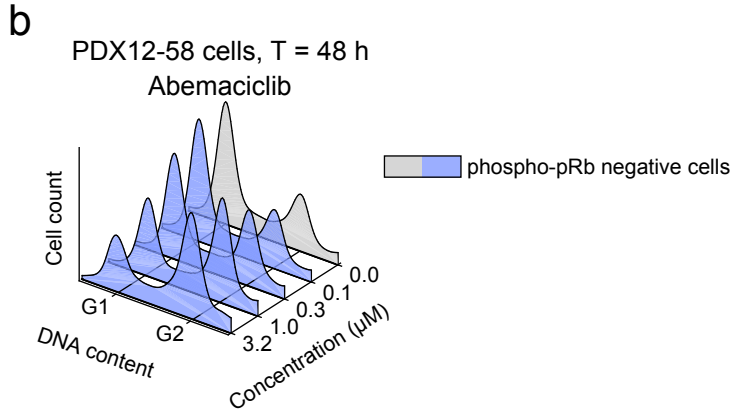

Figure 5

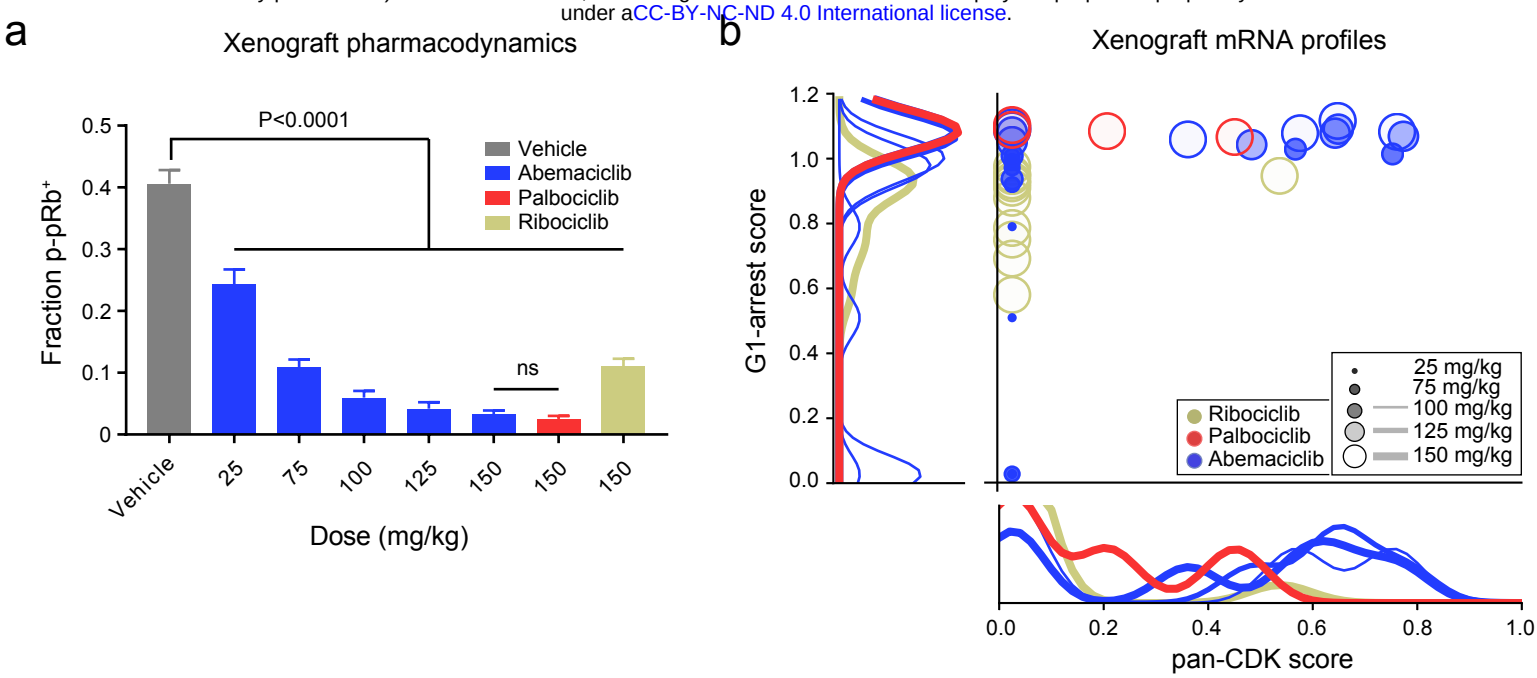

Figure 6

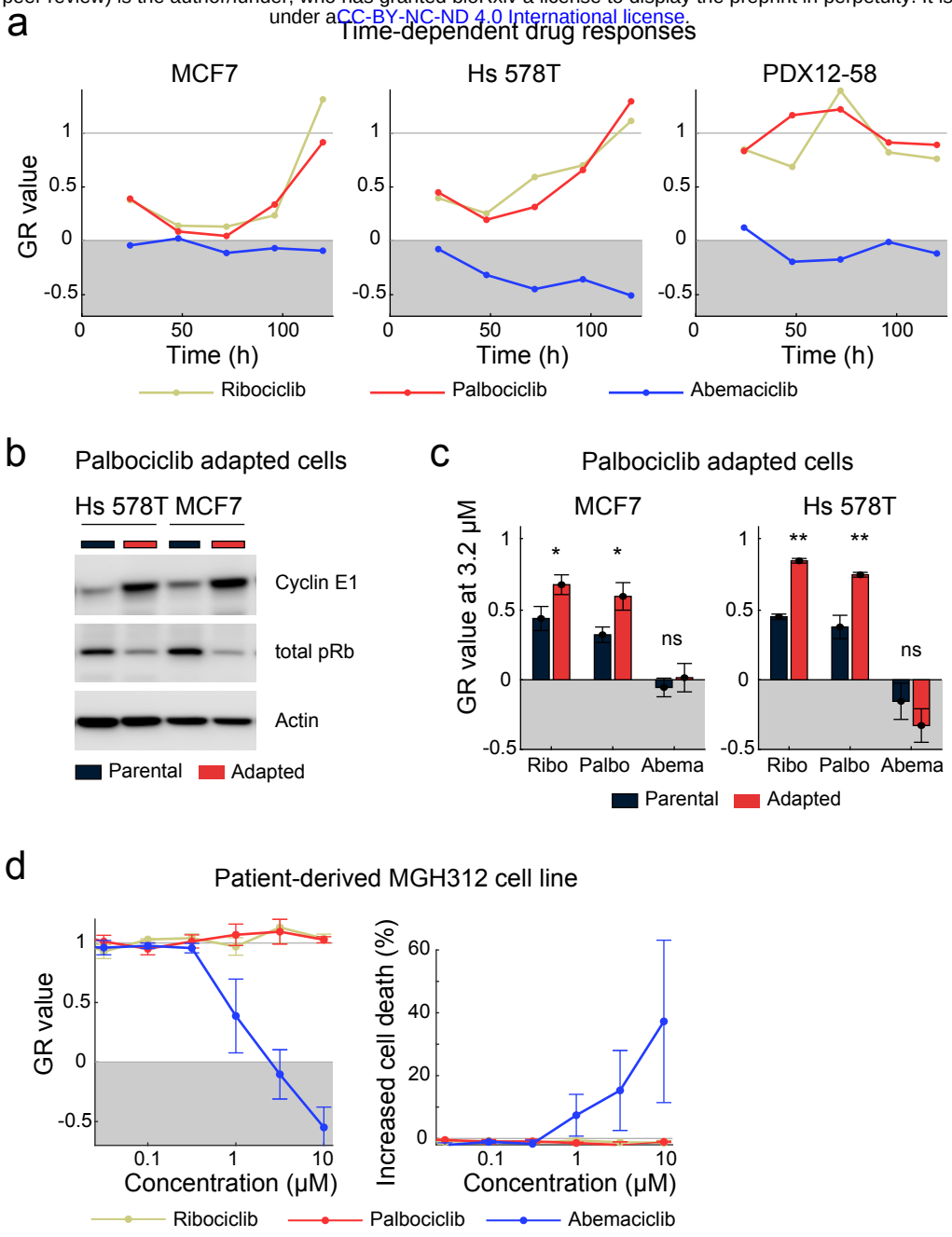

Figure 7

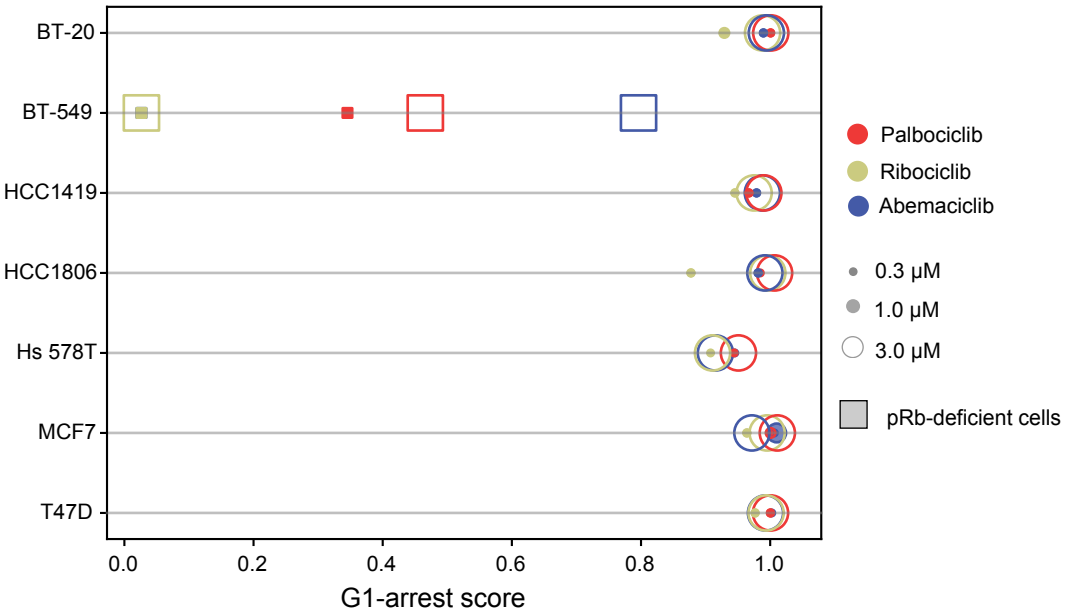

Figure S1. Related to Figure 1.

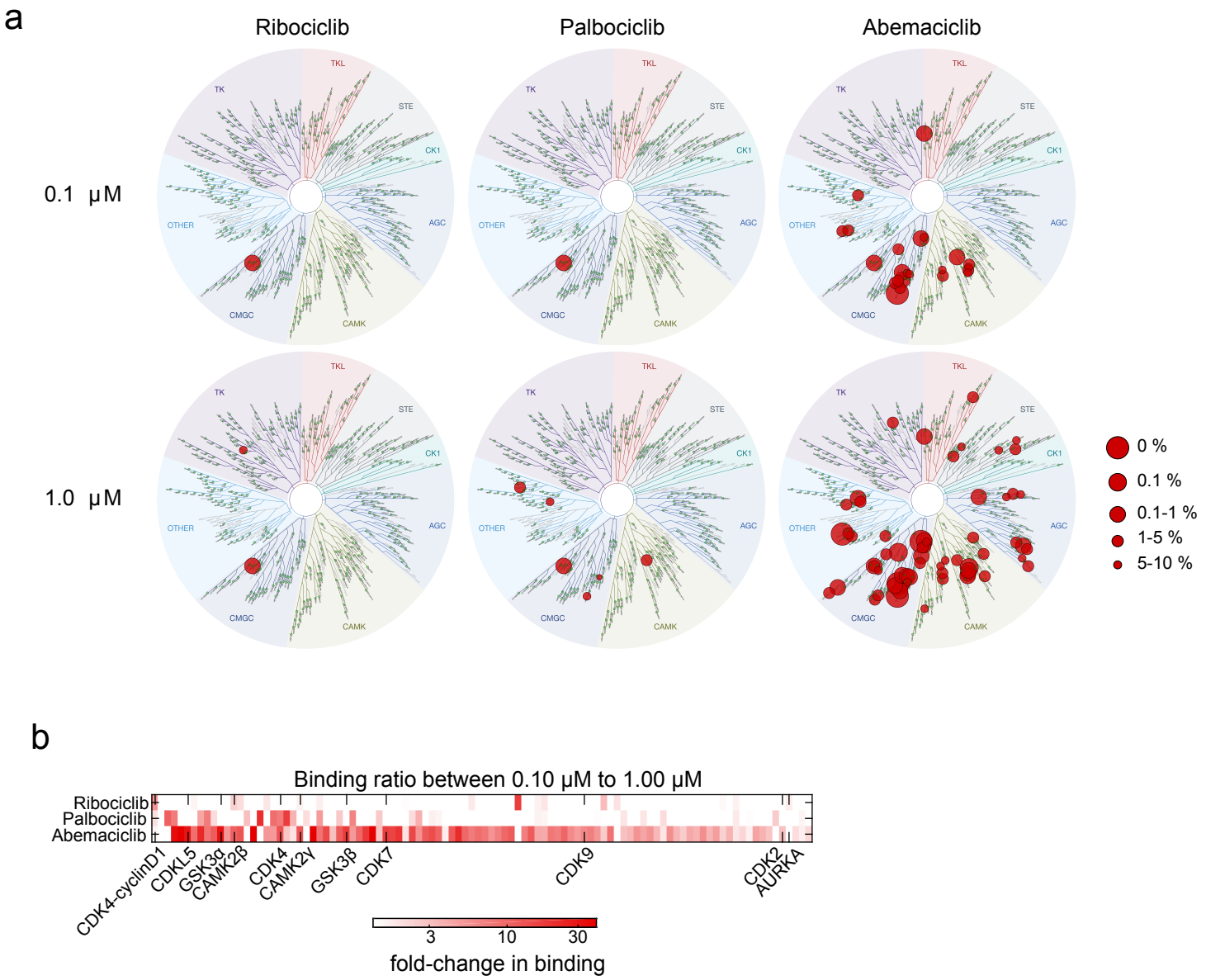

Figure S2. Related to Figure 3.

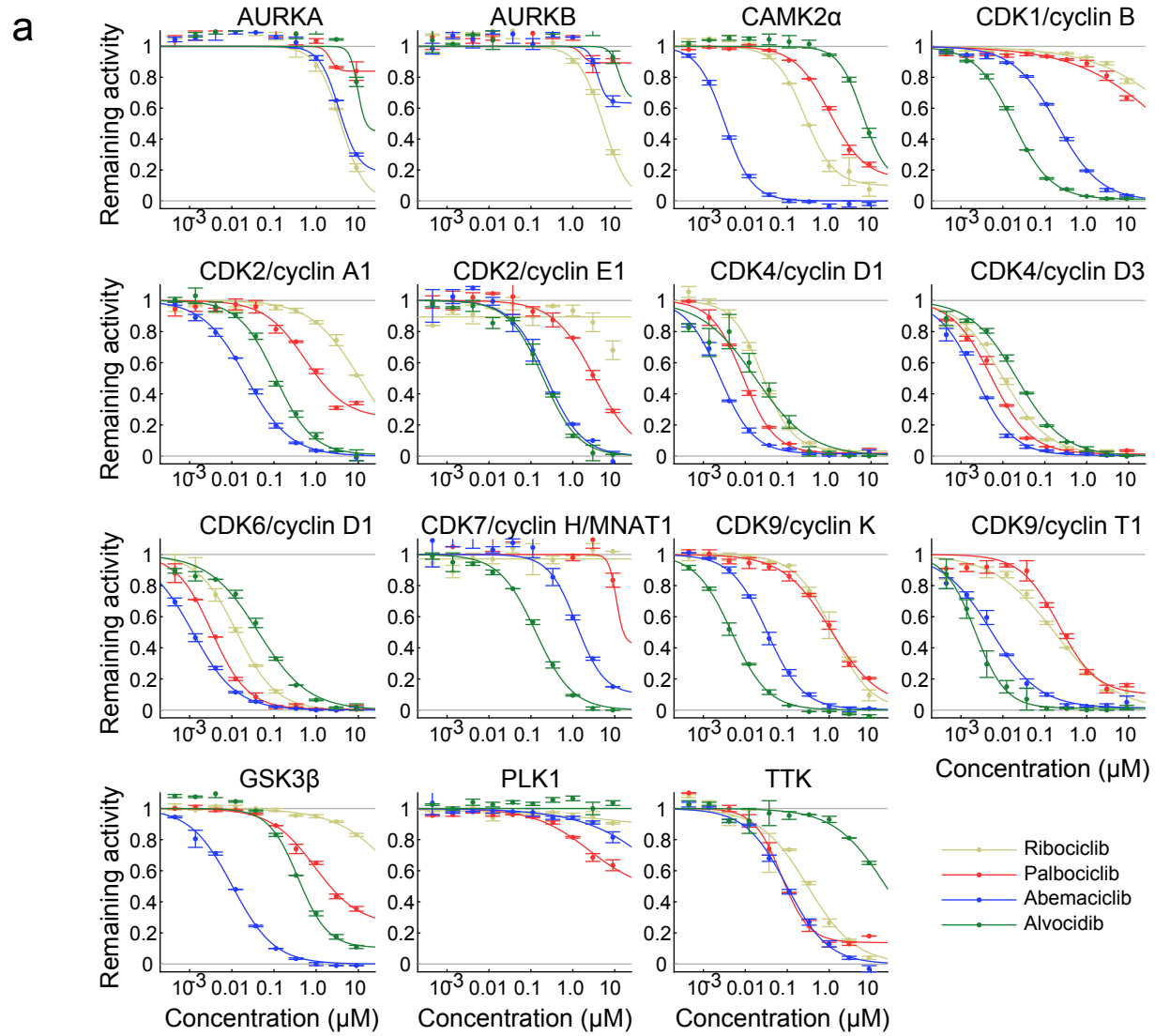

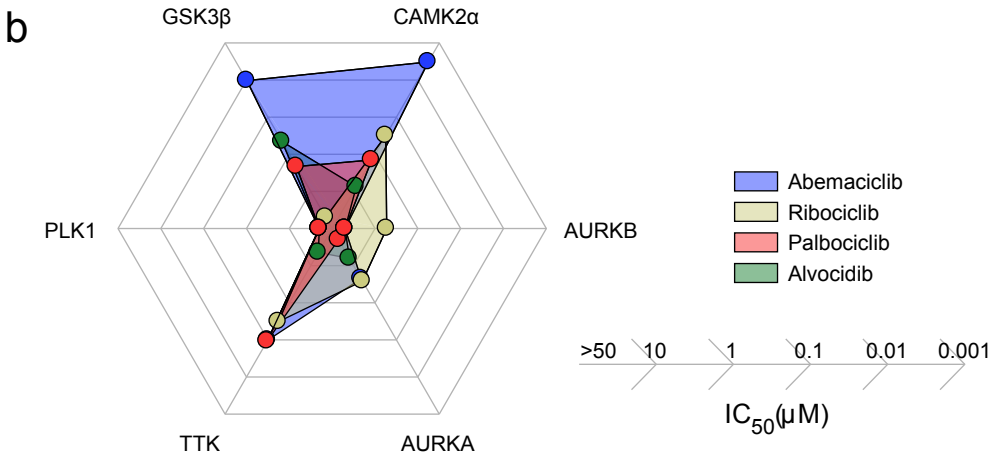

Figure S3. Related to Figure 3.

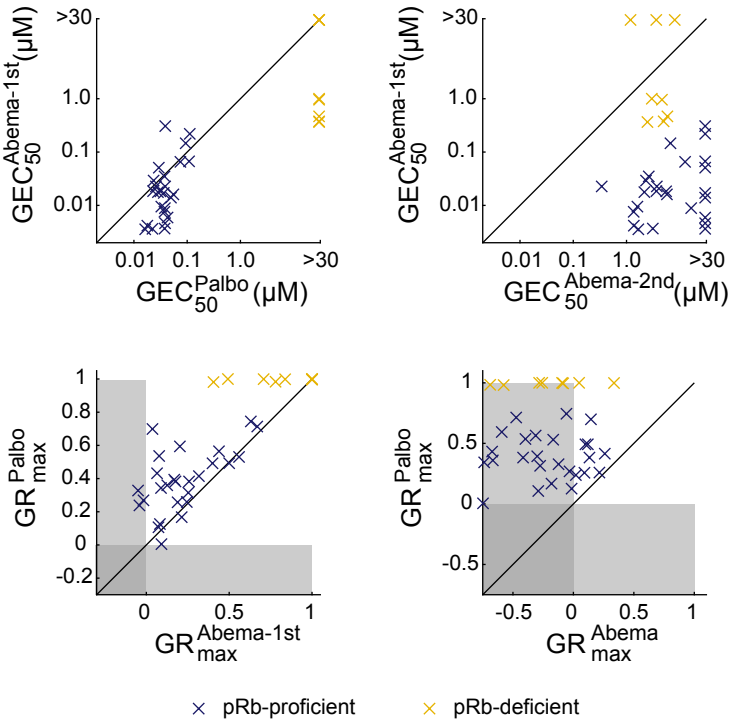

Figure S4. Related to Figure 4.

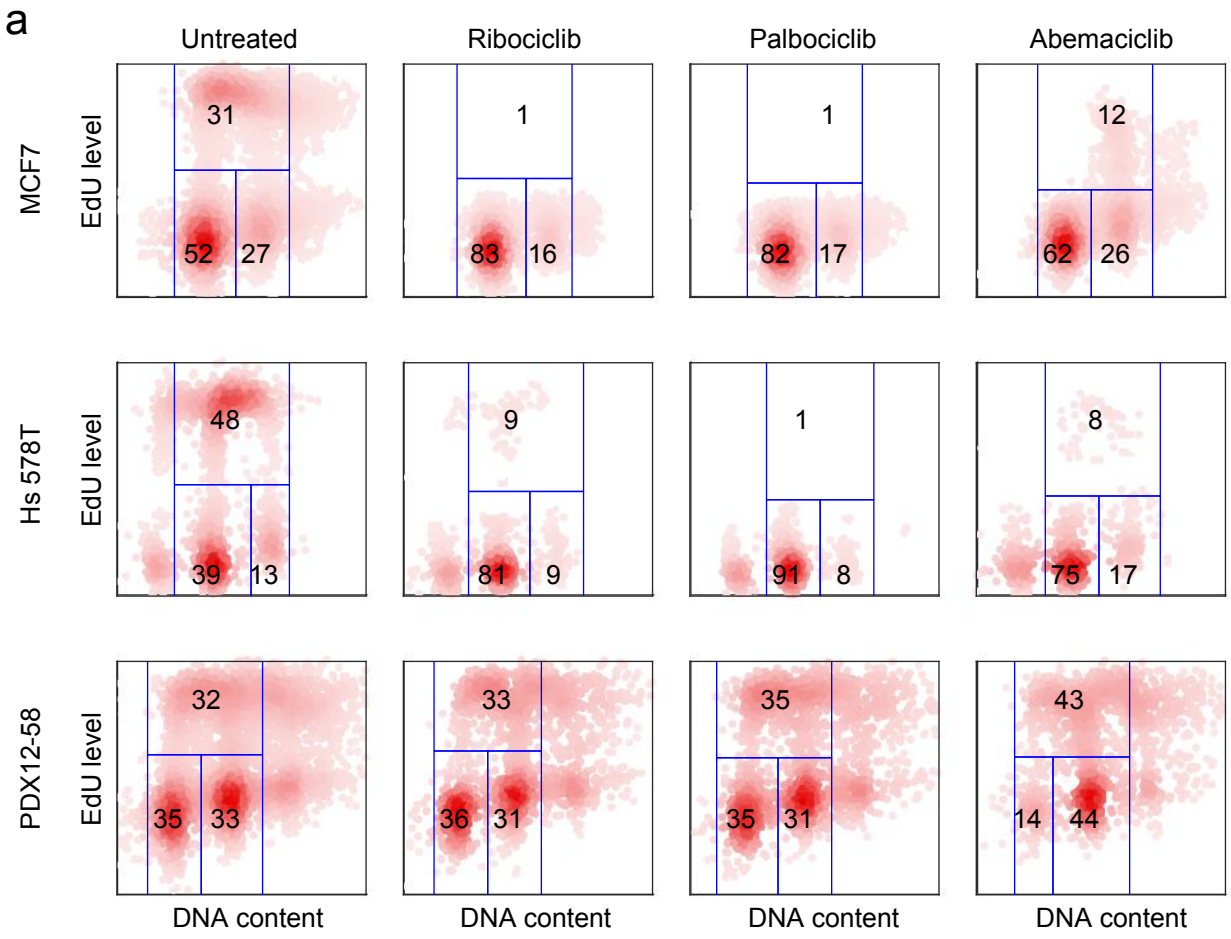

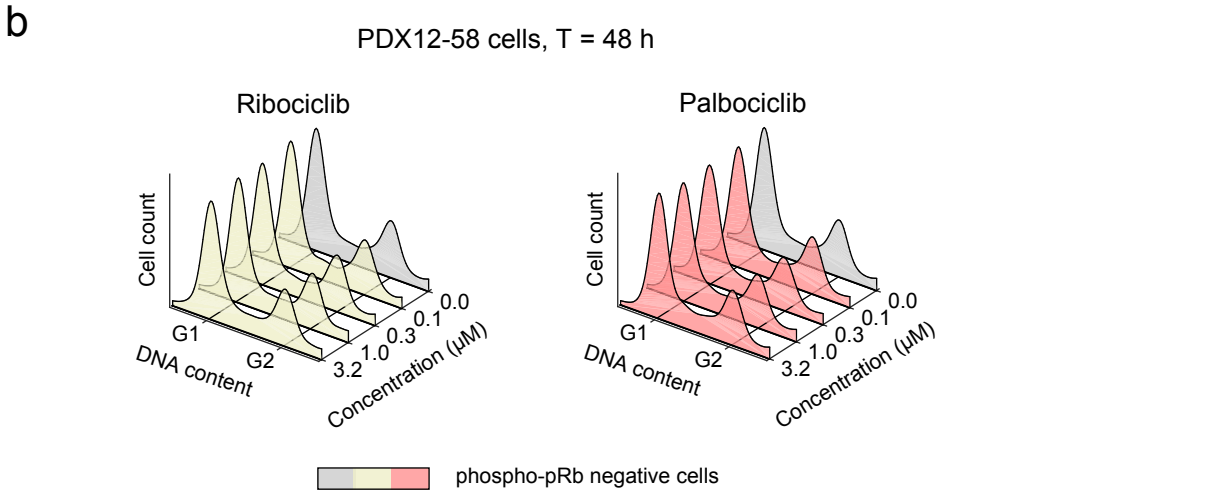

Figure S5. Related to Figure 5.

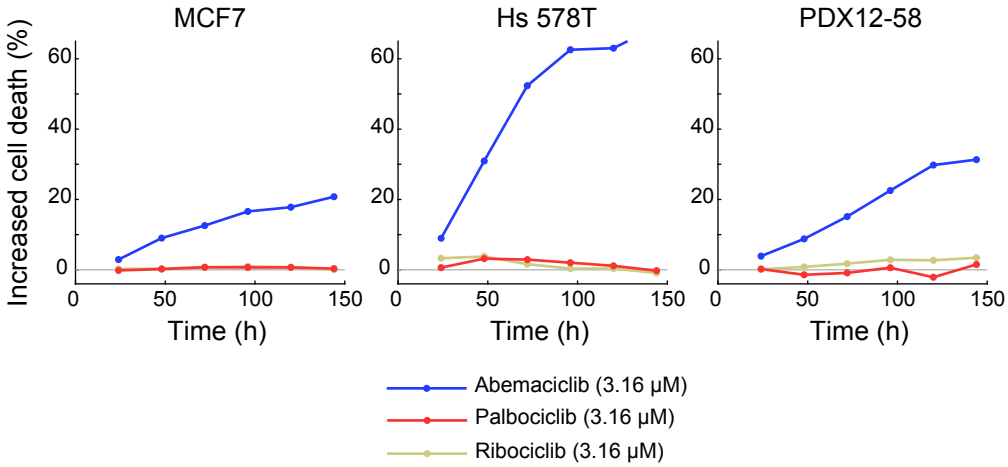

Figure S6. Related to Figure 7.

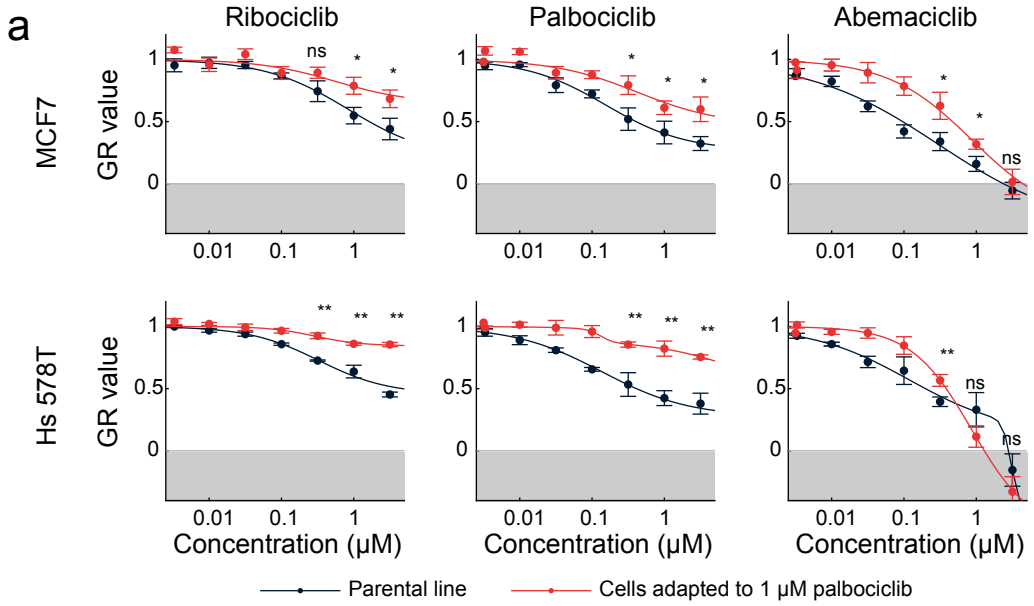

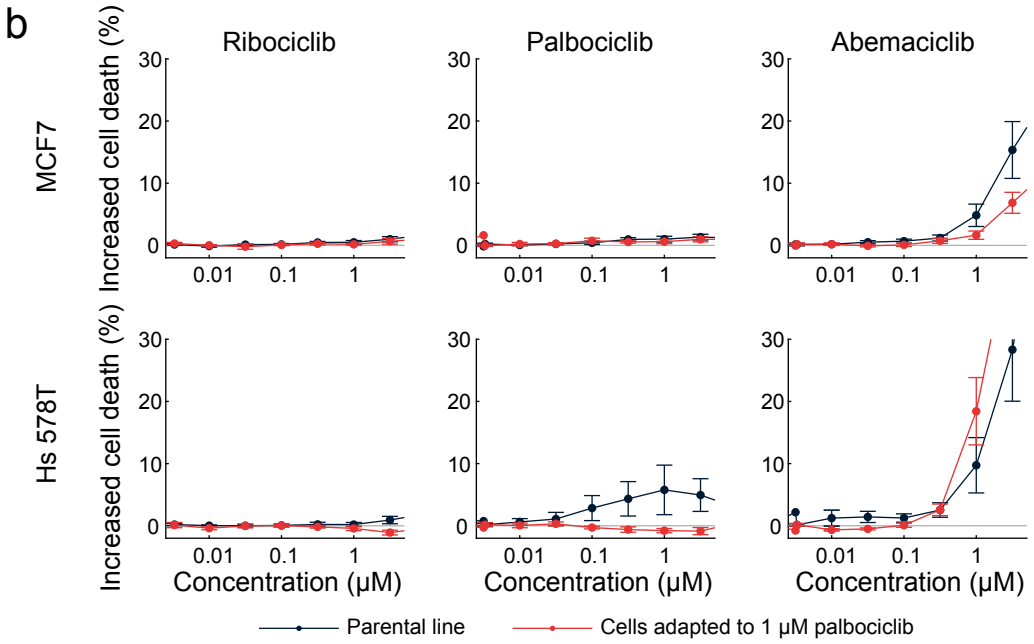

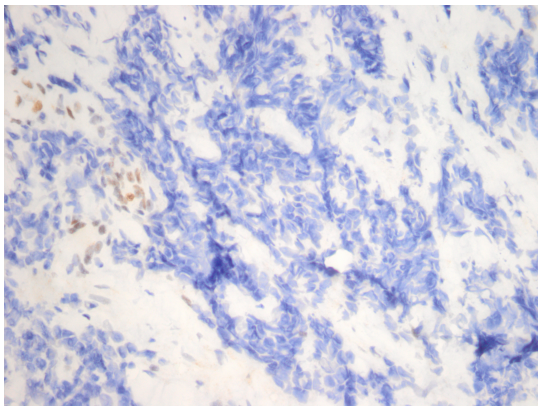

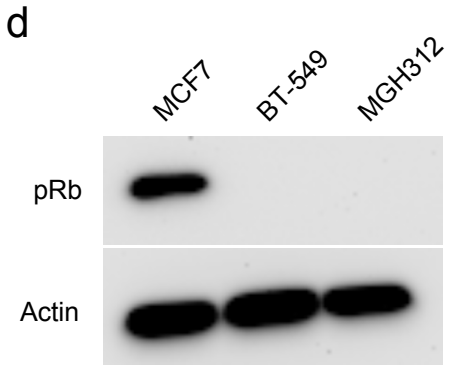

Figure S7. Related to Figure 7.

CONTACT FOR REAGENT AND RESOURCE SHARING

Further information and requests for resources and reagents should be directed to and will be fulfilled by the Lead Contact, Peter Sorger (peter_sorger@hms.harvard.edu).

EXPERIMENTAL MODEL AND SUBJECT DETAILS

Cell lines

All cell lines used in this study were of female human breast cancer origin except the MCF 10A and HME1 cell lines that were derived from non-transformed human breast epithelia. Cell lines were maintained, free of mycoplasma, in their recommended growth conditions listed below, and were identity-validated by STR profiling (Reid *et al.*, 2004).

Cell line	*Growth media*	*Growth conditions*
BT20	EMEM + 10% FBS + 1% P/S	37˚C, 5% CO2
BT549	RPMI-1640 + 10% FBS + 1% P/S, 1 ug/ml IN	37˚C, 5% CO2
CAL120	DMEM + 10% FBS + 1% P/S	37˚C, 5% CO2
CAL51	DMEM + 20% FBS + 1% P/S	37˚C, 5% CO2
CAL851	DMEM + 10% FBS + 1% P/S	37˚C, 5% CO2
CAMA1	EMEM + 10% FBS + 1% P/S	37˚C, 5% CO2
HCC1143	RPMI-1640 + 10% FBS + 1% P/S	37˚C, 5% CO2
HCC1395	RPMI-1640 + 10% FBS + 1% P/S	37˚C, 5% CO2
HCC1419	RPMI-1640 + 10% FBS + 1% P/S	37˚C, 5% CO2
HCC1428	RPMI-1640 + 10% FBS + 1% P/S	37˚C, 5% CO2
HCC1500	RPMI-1640 + 10% FBS + 1% P/S	37˚C, 5% CO2
HCC1806	RPMI-1640 + 10% FBS + 1% P/S	37˚C, 5% CO2
HCC1937	RPMI-1640 + 10% FBS + 1% P/S	37˚C, 5% CO2
HCC1954	RPMI-1640 + 10% FBS + 1% P/S	37˚C, 5% CO2

HCC38	RPMI-1640 + 10% FBS + 1% P/S	37˚C, 5% CO2
HCC70	RPMI-1640 + 10% FBS + 1% P/S	37˚C, 5% CO2
HME1	MEMB + Lonza CC-3150 kit	37˚C, 5% CO2
HS578T	DMEM + 10% FBS + 1% P/S	37˚C, 5% CO2
MCF10A	DMEM/F12 (1:1) + 5% HS + 1% P/S, 20ng/ml EGF, 0.5mg/ml HC, 10 ug/ml IN, 100ng/ml CT	37˚C, 5% CO2
MCF7	DMEM + 10% FBS + 1% P/S	37˚C, 5% CO2
MDAMB157	L-15 + 10% FBS + 1% P/S	37˚C, no CO2
MDAMB231	DMEM + 10% FBS + 1% P/S	37˚C, 5% CO2
MDAMB361	L-15 + 20% FBS + 1% P/S	37˚C, no CO2
MDAMB436	L-15 + 10% FBS + 1% P/S, 10ug/ml IN	37˚C, no CO2
MDAMB453	L-15 + 10% FBS + 1% P/S	37˚C, no CO2
MDAMB468	L-15 + 10% FBS + 1% P/S	37˚C, no CO2
MGH312	RPMI-1640 + 10% FBS + 1% P/S	37˚C, 5% CO2
PDX1258	DMEM/F12 (3:1) + 7.5% FBS + 1% P/S, 0.125ng/ml EGF, 25ng/ml HC, 5ug/ml IN, 8.6ng/ml CT, 5 uM Y-27632 (Palechor-Ceron *et al.*, 2013)	37˚C, 5% CO2
PDX1328	DMEM/F12 (3:1) + 7.5% FBS + 1% P/S, 0.125ng/ml EGF, 25ng/ml HC, 5ug/ml IN, 8.6ng/ml CT, 5 uM Y-27632 (Palechor-Ceron *et al.*, 2013)	37˚C, 5% CO2
PDXHCI002	DMEM/F12 (3:1) + 7.5% FBS + 1% P/S, 0.125ng/ml EGF, 25ng/ml HC, 5ug/ml IN, 8.6ng/ml CT, 5 uM Y-27632 (Palechor-Ceron *et al.*, 2013)	37˚C, 5% CO2
SKBR3	McCoy's + 10% FBS + 1% P/S	37˚C, 5% CO2
SUM1315	F-12 + 5% FBS + 1% P/S, 10ng/ml EGF, 5ug/ml IN, 10mM HEPES	37˚C, 5% CO2
SUM149	F-12 + 5% FBS + 1% P/S, 1ug/ml HC, 5ug/ml IN,	37˚C, 5% CO2

	10mM HEPES	
SUM159	F-12 + 5% FBS + 1% P/S, 1ug/ml HC, 5ug/ml IN, 10mM HEPES	37˚C, 5% CO2
T47D	RPMI-1640 + 10% FBS + 1% P/S, 1 ug/ml IN	37˚C, 5% CO2

Abbreviations: fetal bovine serum (FBS), penicillin/streptomycin (P/S), insulin (IN), hydrocortisone (HC), epidermal growth factor (EGF), cholera toxin (CT). Reagent details can be found in the Key Resources Table.

Animals

Seven week old female NU/NU nude (Crl:NU-Foxn1^{nu}) mice (RRID IMSR_CRL:088) were used for this study (Charles River, Wilmington, MA). The animals were housed five per cage in the Harvard Center for Comparative Medicine animal facility and had *ad libitum* access to food and water (supplemented with 8 µg/ml 17 ß-estradiol to sustain growth of the hormone receptor positive xenografted tumor cells). Once tumors reached 250 mm^3 the mice were randomly assigned to treatment groups. All animal experiments were conducted in accordance with protocols approved by the Institutional Animal Care and Use Committee (IACUC) at Harvard Medical School.

METHOD DETAILS

Dose response measurements

Cells were plated at densities ranging from 500 to 2000 cells per well in 384-well Cell Carrier plates (Perkin Elmer, Waltham, MA) using a Multidrop Combi Reagent Dispenser (Thermo Fisher Scientific, Waltham, MA) and grown for 36 hours. Cells were treated with a dilution series of the indicated drugs by pin transfer or using a D300 Digital Dispenser (Hewlett-Packard, Palo Alto, CA). Drugs were obtained from commercial vendors and tested for purity in-house as described in detail in the HMS LINCS drug collection database (http://lincs.hms.harvard.edu/db/sm/). Cells were stained and fixed for analysis at the time of drug delivery and after 24 to 144 hours of incubation depending on the experiment. Cells were stained at the indicated time points with 2 µg/ml

Hoechst 33342 (Sigma Aldrich, St. Louis, MO) and 1:1000 LIVE/DEAD Far Red Dead Cell Stain (Thermo Fisher Scientific, Waltham, MA) for 30 minutes and fixed with 3.7% formaldehyde (Sigma Aldrich, St. Louis, MO) for 30 minutes. Fixed cells were imaged with a 10x objective using an Operetta microscope and analyzed using the Columbus image data storage and analysis system (Perkin Elmer, Waltham, MA). For most experiments, each condition was tested across three replicate plates and at least four wells per cell line per plate were untreated.

Nuclei counts were normalized to DMSO-treated controls on the same plate to yield relative cell count and normalized growth rate inhibition (GR) values for each technical replicate for each condition (Hafner *et al.*, 2016). Technical replicates were averaged to yield mean relative cell counts and the mean GR value for each condition within each biological replicate. Within each biological replicate, mean GR values for a given cell line / small molecule combination across all tested concentrations were fitted to a biphasic sigmoidal curve with the equation:

$$GR(c) = 2^{\log_2\left(GR_{max}^{1st}+\frac{1-GR_{max}^{1st}}{1+\left(c/GEC_{50}^{1st}\right)^{h^{1st}}}+1\right)\cdot\log_2\left(GR_{max}^{2nd}+\frac{1-GR_{max}^{2nd}}{1+\left(c/GEC_{50}^{2nd}\right)^{h^{2nd}}}+1\right)}-1,$$

or with a single sigmoidal curve with the equation:

$$GR(c) = GR_{max} + \frac{1 - GR_{max}}{1 + \left(c/GEC_{50}\right)^{h}} + 1,$$

or with a flat line with the equation $GR(c) \equiv GR_{max}$. The significance of each curve was assessed using an F-test and the most complex model with $P < 0.05$ was considered to best fit the data. The parameters of the sigmoidal curve and the first phase of the biphasic curve are constrained as described in Hafner *et al*. (Hafner *et al.*, 2017). In the biphasic curve, the parameter GEC_{50}^{2nd} is constrained to be above 0.3 µM. The time-dependent GR values(Hafner *et al.*, 2016) for Figure 7a were evaluated over a 48-hour interval.

Phospho-pRb immunofluorescence and cell cycle analysis

Cells were seeded in 384-well plates, allowed to adhere for 24-36 hours, treated with CDK4/6 inhibitors, incubated for the desired amount of time then fixed in 4%

formaldehyde, permeabilized with 0.5% Triton X-100 in PBS, and blocked with Odyssey blocking buffer (LI-COR, Lincoln, NE). Cells were labeled overnight at 4°C with a 1:800 dilution of anti-phospho-pRb Alexa-555 (Ser807/811) (Cell Signaling Technologies, Danvers, MA) and 2 µg/ml Hoechst 33342 (Sigma Aldrich, St. Louis, MO) prepared in Odyssey blocking buffer. Images were acquired with a Perkin Elmer Operetta microscope as described for the dose response measurements. Nuclei were segmented using Columbus software (Perkin Elmer, Waltham, MA) based on their Hoechst signal. DNA content was defined by the total Hoechst intensity within the nuclear mask. The average phospho-pRb intensity within the nuclear mask was determined, and a threshold for positivity was set by visually inspecting images of several control and treated wells per cell line.

mRNA-seq

Cells were seeded in 12-well plates, and allowed to adhere for 24 hours at which time CDK4/6 inhibitors were added. Cells were lysed in the plates after 6 or 24 hours, and RNA was extracted using Applied Biosystems MagMax 96 total RNA isolation kit (Thermo Fisher Scientific, Waltham, MA) with DNAse digestion according to the manufacturer's protocol. RNA was checked for quantity with a NanoDrop (Thermo Fisher Scientific, Waltham, MA) and for quality using an Agilent Bioanalyzer instrument (with RIN value > 9.0). Libraries were prepared using a TruSeq Stranded mRNA sample preparation kit (Illumina, San Diego, CA) from 500 ng of purified total RNA according to the manufacturer's protocol in a reduced reaction volume. The finished cDNA libraries were assessed for quality using a Bioanalyzer and quantified with a Quant-iT dsDNA Assay kit (Thermo Fisher Scientific, Waltham, MA). The uniquely indexed libraries were multiplexed based on this quantitation and the pooled sample was quantified by qPCR using the Kapa Biosystems (Wilmington, MA) library quantification kit by the Molecular Biology Core Genomics Facility at the Dana-Farber Cancer Institute and sequenced on a single Illumina NextSeq500 run with single-end 75bp reads.

Reads were processed to counts using the bcbio-Nextgen toolkit version 1.0.3a (https://github.com/chapmanb/bcbio-nextgen) as follows: (1) Reads were trimmed and clipped for quality control in cutadapt v1.12; (2) Read quality was checked for each

sample using FastQC 0.11.5; (3) High-quality reads were then aligned into BAM files through STAR 2.5.3a using the human assembly GRCh37; (4) BAM files were imported into DEXSeq-COUNT 1.14.2 and raw counts TPM and RPKM were calculated. R package edgeR (Robinson, McCarthy and Smyth, 2010) 3.18.1 (R version 3.2.1) was used for differential analysis and generate log fold change, *P*-value and FDR.

3'DGE sequencing

Cells were plated at densities ranging from 500 to 2000 cells per well in a 384-well Cell Carrier plate (Perkin Elmer, Waltham, MA) and allowed to adhere for 24 hours. Cells were treated with the CDK4/6 inhibitors, alvocidib, or DMSO using a D300 Digital Dispenser (Hewlett-Packard, Palo Alto, CA). After six hours, the cells were washed once with PBS using an EL405x plate washer (BioTek, Winooski, VT), 10 µl of 1X TCL lysis buffer with 1% (v/v) ß-mercaptoethanol (Qiagen, Hilden, Germany) was added per well, and the plates were stored at -80˚C until the RNA extraction was performed. For RNA extraction, the cell lysate plate was thawed, vortexed briefly, and centrifuged for 1 min at 1000 rpm. Using a BRAVO (Agilent, Santa Clara, CA) liquid handler, the lysate was mixed thoroughly before transferring 10 µl to a 384 well PCR plate. 28 ul of SPRI beads (Beckman Coulter Genomics, Chaska, MN) were added directly to the lysate, mixed and incubated for 5 min. The plate was transferred to a magnetic rack to aggregate the beads, and incubated for 5 min prior to removing the liquid. The beads were washed with 80% ethanol twice, allowed to dry for 1 min, 20 µl of nuclease free water was added per well, the plate was removed from the magnetic rack and the beads were thoroughly resuspended. Following a 5 min incubation, the plate was returned to the magnetic rack and incubated an additional 5 min before transferring the supernatant to a fresh PCR plate. 5 µl of the supernatant was transferred to a separate plate containing RT master mix and 3' and 5' adapters for reverse transcription and template switching (Soumillon *et al.*, 2014), and incubated for 90 min at 42˚C. The cDNA was pooled and purified with a QIAquick PCR purification kit according to the manufacturer's directions with the final elution in 24 µl of nuclease free water. This was followed by an exonuclease I treatment for 30 min at 37˚C that was stopped with a 20 min incubation at 80˚C. The cDNA was then amplified using the Advantage 2 PCR Enzyme System (Takara, Fremont, CA) for 5

cycles, and purified using AMPure XP magnetic beads (Beckman Coulter Genomics, Chaska, MN). Library preparation was completed with 55 ng input using a Nextera DNA kit (Illumina, San Diego, CA) following the manufacturer's instructions, amplified 5 cycles, and purified with AMPure XP magnetic beads (Beckman Coulter Genomics, Chaska, MN). A Pippin PREP purification of the sample from 300-800bp was performed, it was then quantified by qPCR and sequenced on a single Illumina NextSeq run with 75bp paired end reads at the Harvard University Bauer Core Facility.

Reads were processed to counts through the bcbio-nextgen single cell/DGE RNA-seq analysis pipeline (https://bcbio-nextgen.readthedocs.io/en/latest/contents/pipelines.html) a brief description follows: The well barcode and UMIs were identified for all reads and all reads not within one edit distance of a known well barcode were discarded. Each surviving read was quasialigned to the transcriptome (GRCh38) using RapMap (Srivastava *et al.*, 2016). Reads per well were counted using UMIs (Svensson *et al.*, 2017), discarding duplicated UMIs, weighting multimapped reads by the number of transcripts they aligned to and collapsing counts to genes by adding all counts for each transcript of a gene. The R package edgeR 3.18.1 (R version 3.2.1) was used for differential expression analysis.

Clustering analysis of the mRNA-seq data and L1000 signatures

Differential gene expression signatures were clustered along samples and genes based on the cosine distance for the $\log_2$(fold-change) using MATLAB default functions. $\log_2$(fold-change) values for genes with FDR values above 0.2 were set to zero. In Figure 1a, the two down-regulated gene clusters were defined manually based on the dendrogram of the genes. The 'LINCS_L1000_Chem_Pert_down' library obtained from Enrichr (Kuleshov *et al.*, 2016) was used as the reference signature of genes downregulated upon drug perturbation (Table S2). Enrichment analysis was performed on the two down-regulated gene clusters (Figure 1a) against the reference library using the GSEA algorithm (gsea2-2.2.3.jar from the Broad Institute (Subramanian *et al.*, 2005)). Enrichment scores for 31 well-annotated drugs that feature in the library were reported (Figure 1b-c) as $-\log_{10}(P\text{-value})$. G1 and pan-CDK scores for each condition (Figure S1, Figure 1d) were computed as the mean $\log_2$(fold-change) across the genes in

each of the two down-regulated gene clusters identified in Fig 1a. G1 and pan-CDK scores for 3' DGEseq (Figure 2) and MCF7-xenograft mRNAseq (Figure 6b) were computed on the same set of downregulated genes.

Phosphoproteomics mass spectrometry

MCF7 cells were treated with 0.3 μM and 3 μM of palbociclib or abemacicblib or DMSO control for 1 hour in duplicate. For each sample, 4.5 mg of protein was utilized to perform serine and threonine phosphoproteome analysis. The samples were digested using Trypsin (Promega, Madison, WI), acidified and desalted using C18 Sep-Pak (Waters, Milford, MA). Phosphopeptides were enriched using the Thermo Scientific High-Select Fe-NTA Phosphopeptide Enrichment Kit. The samples were labeled using a TMT 10plex Mass Tag Labeling kit (Thermo Fisher Scientific, Waltham, MA) and the reaction was quenched by adding hydroxylamine to a final concentration of 0.5% (v/v) (Kettenbach and Gerber, 2011; Paulo *et al.*, 2015). The sample was then enriched for phosphotyrosine-containing peptides using the pY-1000 antibody (Cell Signaling Technologies, Danvers, MA) coupled to Pierce Protein A Agarose beads (Thermo Fisher Scientific, Waltham, MA). The flow-through from the pY sample was kept and desalted for pS and pT analysis. 24 fractions (phosphoproteomics) were then desalted using the C18 StageTip procedure (Rappsilber, Mann and Ishihama, 2007). All MS analyses were performed on an Orbitrap Fusion Lumos mass spectrometer (Thermo Fisher Scientific, Waltham, MA) using a multi-notch MS3 method(Ting *et al.*, 2011; McAlister *et al.*, 2014). Raw data were converted to mzXML and searched via Sequest (Eng, McCormack and Yates, 1994) version 28 against a concatenated Uniprot database (downloaded 02/04/2014). Linear discriminate analysis was used to distinguish forward and reverse hits and reverse hits were filtered to an FDR of 1% at the protein level. Site localization confidence was assessed using the A-score method (Beausoleil *et al.*, 2006). Reporter ion intensities were quantified and normalized as described earlier (Paulo *et al.*, 2015).

Annotation of phosphopeptides with upstream kinases

16,300 phosphopeptides were detected across all conditions in MCF7 cells. The PhosphoSitePlus (PSP) database (Hornbeck *et al.*, 2012), which contains curated annotations of upstream kinases, was queried using phosphopeptide sequence motifs and

UniProt IDs as identifiers. Only ~6.3% of the phosphopeptides detected by phosphoproteomics had experimentally verifiable kinase annotations on PSP. The NetworKIN algorithm (Horn *et al.*, 2014) that predicts upstream kinases, based on phosphopeptide sequences and STRING evidence, was used to identify kinases for the remaining phosphosites. A further 14% of phosphosites were annotated with predicted kinases (NetworKIN Score > 4). In total, 3145 phosphopeptides from 1242 proteins were annotated as being phosphorylated by 365 kinases (8297 kinase-peptide interaction pairs).

Differential kinase activity score using GSEA

Based on the method described previously (Drake *et al.*, 2012), a custom python package was developed to infer differential kinase activity across drug treatments (https://github.com/datarail/msda). A kinase set library was assembled using the identified kinase-substrate relationships. The kinase set library is composed of kinases and their corresponding sets of phosphopeptide substrates. Only kinase sets that had more than 25 downstream phosphosites were used. The final kinase set library was composed of 60 kinases that phosphorylate 2597 peptides. For each phosphopeptide, the mean difference between the replicates and the maximum difference across conditions were computed. If the delta between the two scores was less than 1, then the phosphopeptide measurement was considered noisy and discarded, resulting in a final list of 9958 phosphopeptides (Table S4). For each of the four treatment conditions, the average log2 (fold-change) was computed relative to the untreated control. Using the phosphopeptide log2(fold-change) values as input and the final kinase set library, GSEA algorithm (gsea2-2.2.3.jar from Broad Institute (Subramanian *et al.*, 2005)) was used to infer the enrichment score ($P < 0.05$ and FDR < 0.2). The enrichment score is a proxy metric for the differential activity of the kinases.

Measurement of kinase inhibition with kinobeads

Multiplex inhibitor beads (MIB) (Duncan *et al.*, 2012) were generously provided by Gary Johnson (University of North Carolina). A mixed cell lysate comprised of K562, COLO0205, SK-N-BE(2), MV-4-11 cells was prepared as previously described (Médard

et al., 2015), and clarified by filtration through 0.45 µm and 0.22 µm filters. 3 mg of the mixed cell lysate was treated with CDK4/6 inhibitors or DMSO overnight at 4˚C with continuous rocking. The samples were enriched for kinases by passing them through a sepharose bead column followed by a MIB column. The samples were washed with MIB wash buffer (50 mM HEPES pH 7.5, 0.5% Triton X-100, 1 mM EDTA, 1 mM EGTA) with high (1 M NaCl) and low (150 mM NaCl) salt, and then in low salt MIB buffer containing 0.1% SDS (w/v). Kinases bound to the MIBs were eluted twice with 500 µl/column of MIB elution buffer (0.5% (w/v) SDS, 10 µM DTT, 0.1 M Tris-HCl pH 6.8). The eluent was boiled for 15 min at 97˚C, and alkylated with 0.5 M iodoactamide (30 µl per ml of sample) for 30 min at room temperature. The samples were precipitated with tricholoracetic acid (25% final volume), washed twice with methanol, and dried. The samples were solubilized in 8 M urea in 20 mM EPPS. Additional EPPS was added to decrease the concentration of urea to 2 M prior to adding acetonitrile (ACN) and lysC (2 µg/µl) for 3 hours at room temperature. The samples were digested with trypsin (0.5 µg/µl) overnight at 37˚C. Additional ACN was added, followed by 5 µl of tandem mass tag (TMT) labels (Thermo Fisher Scientific, Waltham, MA) for 1 hour at room temperature. At this stage a ratio check was performed to ensure equal loading of each individually TMT-labeled sample, and to check the efficiency of the labeling reaction. The labeling reactions were quenched with 5 µl of 10% hydroxylamine for 10 min at room temperature, at which point the samples were pooled, diluted with 100% formic acid, evaporated to 0.5 ml, diluted with 1% formic acid, and then desalted by passing through a solid phase extraction cartridge (Thermo Fisher Scientific, Waltham, MA). Samples were eluted in 70% ACN and 1 % formic acid, evaporated, and reconstituted in 300 µl of 0.1% TFA. The samples were analyzed on an Orbitrap Fusion Lumos mass spectrometer. Peptide intensities of the proteins pulled down by the MIBs were summed to obtain total protein intensities. The protein intensities were normalized using the iBAQ method (Schwanhäusser *et al.*, 2011). For each treatment condition, log2(fold-change) values were computed relative to untreated (DMSO) control.

In vitro measurement of kinase inhibitory activity

Ribociclib, palbociclib, and abemaciclib were assayed using the KINOMEscan® assay platform (DiscoverX, Fremont, CA). Data are reported as percent of remaining activity at

either 0.1 or 1.0 μM drug concentration. The activity of ribociclib, palbociclib, abemaciclib, and alvocidib on multiple CDK-cyclin complexes and other kinases were assayed using Thermo Fisher Scientific SelectScreen Kinase Profiling service. The 'Adapta™' assay was used for CDK4/cyclin D1, CDK4/cyclin D3, CDK6/cyclin D1, CDK7/cyclin H/MNAT1, and CDK9/cyclin T1. The 'LanthaScreen™' Kinase Binding assay was used for CDK2/cyclin A1, CDK2/cyclin E1, CDK9/cyclin K, and TTK. The 'Z′-LYTE™' assay was used for CDK1/cyclin B, AURKA, AURKB, CAMK2A, GSK3B, and PLK1. The ATP concentration was Km[app] when available or 10 μM otherwise.

Western blots

20 μg of whole cell lysate (Figure 7b) or 12 μg of whole cell lysate (Figure S7), prepared in M-PER lysis buffer (Thermo Fisher Scientific, Waltham, MA) with complete protease inhibitor cocktail (Sigma Aldrich, St. Louis, MO), was added per well in Mini-PROTEAN TGX precast gels (Bio-Rad, Hercules, CA). Primary mouse monoclonal pRb, cyclin E, and β-actin antibodies were used at 1:1000 dilutions. Secondary anti-mouse IgG, HRP-linked was used 1:2000. All antibodies were from Cell Signaling Technologies (Danvers, MA).

Immunohistochemistry

A 4 μm slice of a formalin-fixed, paraffin-embedded, biopsy of the liver lesion from which the MGH312 cell line was derived was mounted on a standard glass slide and stained for RB expression using a Leica Bond autostainer. The primary Rb antibody (clone 1F8; Bio SB, Santa Barbara, CA) was diluted 1:500 in Leica Bond Diluent and incubated for 15 min. The slide was counterstained with hematoxylin.

Identifying genes associated with differential efficacy of abemaciclib and palbociclib

Using the baseline mRNA expression of 30 genes linked to the cell cycle (cyclins, CDKs, CDKLs, and CDKNs), we built a multilinear model (MATLAB function 'fitglm') to predict the difference in GR values at 3.16 μM between palbociclib and abemaciclib for the pRb-proficient cell lines profiled in Figure 4a. Predictors with non-significant coefficients ($P > 0.05$) were iteratively removed until only significant coefficients

remained. A leave-one-out cross validation was performed with the remaining predictors to yield the results in Figure 4c. Note that results were qualitatively similar if the pRb-deficient cell lines were included.

In vivo studies

Thirty-five seven-week-old NU/NU nude mice (Charles River Laboratories, Wilmington, MA) were supplemented with 8 µg/ml 17ß-estradiol (Sigma Aldrich, St. Louis, MO) by adding it to their drinking water five days prior to tumor engraftment, and replacing it twice per week. Mice were engrafted with 5 x 10^6 MCF-7 cells 1:1 in growth factor reduced matrigel (Corning, Corning, NY) subcutaneously in each flank, and allowed to grow to ~300 mm^3. The animals were then randomly assigned to treatment groups, and treated daily for four days with ribociclib (150 mg/kg), palbociclib (150 mg/kg), abemaciclib (25, 75, 100, 125, or 150 mg/kg), or vehicle control (0.5% (w/v) hydroxyethyl cellulose (Sigma Aldrich, St. Louis, MO) and 0.05% (v/v) antifoam (Sigma Aldrich, St. Louis, MO) in water) by oral gavage. Animals were sacrificed two hours after receiving the last dose. The tumors were excised and cut in half, one half was fixed in 4% formaldehyde at 4˚C and transferred to 0.1% sodium azide after 48 hours, the other flash frozen, and a thin slice from the center of the tumor was placed in RNA*later* at 4˚C (Qiagen, Hilden, Germany), after 48 hours the RNA*later* was aspirated, and samples were transferred to -80˚C.

The fixed tumor samples were paraffin-embedded at the Harvard Medical Area Rodent Histopathology Core and a tissue microarray (TMA) was constructed at the Tissue Microarray & Imaging Core by arraying three 1 mm cores per sample in a block. Sequential 5 µm slices were mounted on superfrost slides. The slides were subjected to manual dewaxing and antigen retrieval as described previously (Lin *et al.*, 2017). The slides were then blocked with Odyssey buffer (LI-COR, Lincoln, NE) and pre-stained with secondary antibodies prior to beginning cyclic immunofluorescence (Lin *et al.*, 2017). The antibodies used in this study are listed in the Key Resources Table. Images were acquired on a RareCyte CyteFinder (Seattle, WA) slide scanning microscope with a 10X 0.3 NA objective. Image quantitation was performed in ImageJ as previously

described (Lin *et al.*, 2017). Human cells were distinguished from mouse cells based on e-cadherin and vimentin intensities, and only the e-cadherin-high, vimentin-low cells were included in subsequent analyses. A threshold for phospho-pRb positive cells was set manually by comparing the intensity distributions of phospho-pRb staining in tumors from mice that received the vehicle control and 150 mg/kg palbociclib.

The RNA*later* preserved samples were thawed on ice, 600 µl of RLT with 10% 2-mercaptoethanol was added and the tumors were manually dissociated with microfuge pestles (Thomas Scientific, Swedesboro, NJ). Samples were passed through QiaShredder columns, and then loaded on RNeasy columns (Qiagen, Hilden, Germany) and processed according to the manufacturer's specifications with a 30 min incubation in DNase. Library preparation, and analysis were performed as described in section 4. A single Illumina NextSeq500 run with single-end 75bp reads was performed at the Harvard Medical School Biopolymers Facility. Reads were processed as described in section 4, with the additional step that the alignment algorithm identified and excluded reads that aligned with the mouse genome to ensure that downstream analyses were performed on the xenograft transcripts only. Non-coding genes were excluded from the transcript per million (TPM) counts table and Principal Component Analyses (PCA) was performed. For each treated sample, the fold-change of transcripts relative to vehicle control was computed using edgeR (Robinson, McCarthy and Smyth, 2010). G1 and pan-CDK scores were computed as described in section 6.

QUANTIFICATION AND STATISTICAL ANALYSIS

Image quantification was performed with Columbus (Perkin Elmer, Waltham, MA) software. All subsequent analyses were performed using MATLAB and python. All relevant statistical details are included in the figure captions, and text. Additional details for each experiment type are included in the METHOD DETAILS section of the STAR Methods.

DATA AND SOFTWARE AVAILABILITY

The RNA sequencing data sets related to Figures 1, 2, and 6 have been deposited on GEO, and can be found under accession numbers GSE99116, pending and pending respectively. The phosphoproteomics data set related to Figure 3 is freely available on Synapse, ID syn11622501, https://www.synapse.org/#!Synapse:syn11622501. The dose response data sets related to Figure 4 are available in the HMS LINCS database, IDs 20343 and 20344, http://lincs.hms.harvard.edu/db/datasets/20343/ http://lincs.hms.harvard.edu/db/datasets/20344/.

KEY RESOURCES TABLE

REAGENT or RESOURCE	SOURCE	IDENTIFIER
Antibodies		
Phospho-pRb (Ser807/811) (clone D20B12) Alexa 555	Cell Signaling Technologies	Cat # 8957; RRID AB_2728827
pRb (clone 4H1)	Cell Signaling Technologies	Cat # 9309; RRID AB_823629
Cyclin E1 (clone HE12)	Cell Signaling Technologies	Cat # 4129; RRID AB_2071200
β-Actin (clone 8H10D10)	Cell Signaling Technologies	Cat # 3700; RRID AB_10985704
Anti-mouse IgG, HRP-linked	Cell Signaling Technologies	Cat # 7076; RRID AB_330924
Vimentin (clone D21H3) Alexa 555	Cell Signaling Technologies	Cat # 9855; RRID AB_10859896
E-cadherin (clone 24E10) Alexa 488	Cell Signaling Technologies	Cat # 3199; RRID AB_823441
Chemicals, Peptides, and Recombinant Proteins		
Palbociclib	MedChem Express	Cat # HY-50767, batch # 16349
Abemaciclib	MedChem Express	Cat # HY-16297, batch # 08492
Ribociclib	MedChem Express	Cat # HY-15777, batch # 11003
Alvocidib	Haoyuan chemexpress	Cat # HY-10005, batch # HY-009_TM-20090429
Fetal bovine serum	Life Technologies	26140-079
Horse Serum	Life Technologies	16050-122
Penicillin/Streptomycin	Corning	30-002-Cl

Epidermal growth factor	PeproTech	AF-100-15
Insulin	Sigma Aldrich	I1882
Hydrocortisone	Sigma Aldrich	H0888
Cholera toxin	Sigma Aldrich	C8052
Y-27632	Enzo Life Sciences	ALX-270-333-M025
Critical Commercial Assays		
KINOMEscan	DiscoverX	SCANmax
SelectScreen Z' lyte	Life Technologies	Z'Lyte
SelectScreen Lantha	Life Technologies	Lantha
SelectScreen Adapta	Life Technologies	Adapta
TruSeq kit	Illumina	Cat # 20019792
Deposited Data		
mRNAseq on cell lines	This paper	GEO GSE99116
Phosphoproteomics	This paper	Synapse syn11622501
Dose response	This paper	LINCS DB 20343, 20344
3' DGEseq on cell lines	This paper	GEO pending
mRNAseq on xenografts	This paper	GEO pending
Experimental Models: Cell Lines		
BT20	ATCC	HTB-19; RRID CVCL_0178
BT549	ATCC	HTB-122; RRID CVCL_1092
CAL120	DSMZ	ACC 459; RRID CVCL_1104
CAL51	DSMZ	ACC 302; RRID CVCL_1110
CAL851	DSMZ	ACC 440; RRID CVCL_1114
CAMA1	ATCC	HTB-21; RRID CVCL_1115
HCC1143	ATCC	CRL-2321; RRID CVCL_1245
HCC1395	ATCC	CRL-2324; RRID CVCL_1249
HCC1419	ATCC	CRL-2326; RRID CVCL_1251
HCC1428	ATCC	CRL-2327; RRID CVCL_1252
HCC1500	ATCC	CRL-2329; RRID CVCL_1254
HCC1806	ATCC	CRL-2335; RRID CVCL_1258

HCC1937	ATCC	CRL-2336; RRID CVCL_0290
HCC1954	ATCC	CRL-2338; RRID CVCL_1259
HCC38	ATCC	CRL-2314; RRID CVCL_1267
HCC70	ATCC	CRL-2315; RRID CVCL_1270
HME1	ATCC	CRL-4010; RRID CVCL_3383
HS578T	ATCC	HTB-126; RRID CVCL_0332
MCF10A	ATCC	CRL-10317; RRID CVCL_0598
MCF7	ATCC	HTB-22; RRID CVCL_0031
MDAMB157	ATCC	HTB-24; RRID CVCL_0618
MDAMB231	ATCC	HTB-26; RRID CVCL_0062
MDAMB361	ATCC	HTB-27; RRID CVCL_0620
MDAMB436	ATCC	HTB-130; RRID CVCL_0623
MDAMB453	ATCC	HTB-131; RRID CVCL_0418
MDAMB468	ATCC	HTB-132; RRID CVCL_0419
MGH312	MGH (Crystal *et al.*, 2014)	
PDX1258	Brugge lab	
PDX1328	Sorger lab	
PDXHCI002	Brugge lab	
SKBR3	ATCC	HTB-30; RRID CVCL_0033
SUM1315	University of Michigan	SUM-1315MO2; RRID CVCL_5589
SUM149	Asterand	SUM-149PT; RRID CVCL_3422
SUM159	Asterand	SUM-159PT; RRID CVCL_5423
T47D	ATCC	HTB-133; RRID CVCL_0553

Software and Algorithms		
MATLAB (R2016b)	MathWorks	https://www.mathworks.com/products/matlab.html
Columbus (v2.7.0)	Perkin Elmer, Waltham, MA	http://www.perkinelmer.com/product/image-data-storage-and-analysis-system-columbus
bcbio-Nextgen toolkit (v1.0.3a)		https://github.com/chapmanb/bcbio-nextgen
edgeR v3.18.1 (R v3.2.1)	(Robinson, McCarthy and Smyth, 2010; McCarthy, Chen and Smyth, 2012)	https://bioconductor.org/packages/release/bioc/html/edgeR.html
Sequest (v28)	(Eng, McCormack and Yates, 1994)	http://fields.scripps.edu/yates/wp/
Kinase activity inference		https://github.com/datarail/msda